OCT 14 1992

ORNL
MASTER COPY

NUREG/CR-6003
ORNL/TM-12130

Density-Wave Instabilities in Boiling Water Reactors

Prepared by
J. March-Leuba

Oak Ridge National Laboratory

Prepared for
U.S. Nuclear Regulatory Commission

AVAILABILITY NOTICE

Availability of Reference Materials Cited in NRC Publications

Most documents cited in NRC publications will be available from one of the following sources:

1. The NRC Public Document Room, 2120 L Street, NW., Lower Level, Washington, DC 20555

2. The Superintendent of Documents, U.S. Government Printing Office, P.O. Box 37082, Washington, DC 20013-7082

3. The National Technical Information Service, Springfield, VA 22161

Although the listing that follows represents the majority of documents cited in NRC publications, it is not intended to be exhaustive.

Referenced documents available for inspection and copying for a fee from the NRC Public Document Room include NRC correspondence and internal NRC memoranda; NRC bulletins, circulars, information notices, inspection and investigation notices; licensee event reports; vendor reports and correspondence; Commission papers; and applicant and licensee documents and correspondence.

The following documents in the NUREG series are available for purchase from the GPO Sales Program: formal NRC staff and contractor reports, NRC-sponsored conference proceedings, international agreement reports, grant publications, and NRC booklets and brochures. Also available are regulatory guides, NRC regulations in the *Code of Federal Regulations*, and *Nuclear Regulatory Commission Issuances*.

Documents available from the National Technical Information Service include NUREG-series reports and technical reports prepared by other Federal agencies and reports prepared by the Atomic Energy Commission, forerunner agency to the Nuclear Regulatory Commission.

Documents available from public and special technical libraries include all open literature items, such as books, journal articles, and transactions. *Federal Register* notices, Federal and State legislation, and congressional reports can usually be obtained from these libraries.

Documents such as theses, dissertations, foreign reports and translations, and non-NRC conference proceedings are available for purchase from the organization sponsoring the publication cited.

Single copies of NRC draft reports are available free, to the extent of supply, upon written request to the Office of Administration, Distribution and Mail Services Section, U.S. Nuclear Regulatory Commission, Washington, DC 20555.

Copies of industry codes and standards used in a substantive manner in the NRC regulatory process are maintained at the NRC Library, 7920 Norfolk Avenue, Bethesda, Maryland, for use by the public. Codes and standards are usually copyrighted and may be purchased from the originating organization or, if they are American National Standards, from the American National Standards Institute, 1430 Broadway, New York, NY 10018.

DISCLAIMER NOTICE

This report was prepared as an account of work sponsored by an agency of the United States Government. Neither the United States Government nor any agency thereof, or any of their employees, makes any warranty, expressed or implied, or assumes any legal liability of responsibility for any third party's use, or the results of such use, of any information, apparatus, product or process disclosed in this report, or represents that its use by such third party would not infringe privately owned rights.

NUREG/CR-6003
ORNL/TM-12130

Density-Wave Instabilities in Boiling Water Reactors

Manuscript Completed: June 1992
Date Published: September 1992

Prepared by
J. March-Leuba

Oak Ridge National Laboratory
Managed by Martin Marietta Energy Systems, Inc.

Oak Ridge National Laboratory
Oak Ridge, TN 37831-6285

Prepared for
Division of Systems Technology
Office of Nuclear Reactor Regulation
U.S. Nuclear Regulatory Commission
Washington, DC 20555
NRC FIN L1697

ABSTRACT

This report contains a review of issues related to density-wave instabilities in boiling water reactors (BWRs). The report describes the types of instability modes that can be expected in operating reactors; these modes are (1) the channel thermohydraulic instability mode, (2) the core-wide instability mode, and (3) the out-of-phase instability mode. The physical mechanisms leading to each type of instability are reviewed and documented, along with some common mathematical models used in stability calculations. The main approximations used in these mathematical models are presented, and their impact on the accuracy of the calculations is reviewed. The linear behavior of a BWR is studied through the use of transfer functions, and the nonlinear behavior and limit cycle development are studied. A summary of the sensitivities to physical parameters is also included in this report.

CONTENTS

Page

ABSTRACT iii

LIST OF FIGURES vi

LIST OF TABLES vii

1 Introduction 1

2 Types of Instabilities Observed in BWRs 2
- 2.1 Control System Instabilities 2
- 2.2 Channel Thermohydraulic Instabilities 2
- 2.3 Coupled Neutronic-Thermohydraulic Instabilities 4

3 Physical Mechanisms Leading to Instabilities in BWRs 8
- 3.1 The Density-Wave: Flow Oscillations 8
- 3.2 Neutronic Feedback During Oscillations 10
- 3.3 Boundary Conditions for Different Oscillation Modes 12

4 Mathematical Models for BWR Stability Calculations 16
- 4.1 Numerical Approximations for the Solution of Partial Differential Equations 16
  - 4.1.1 Nodal Approximations 16
  - 4.1.2 Modal Approximations 16
- 4.2 BWR Neutron Dynamics 17
  - 4.2.1 Reactivity Feedback in the Point Kinetics Formalism 17
  - 4.2.2 Thermohydraulic Feedback in Multidimensional Diffusion Calculations 19
- 4.3 BWR Thermohydraulics 21
- 4.4 Mode Orthogonality: Excitation of the First Axial Harmonic 21

5 BWR Linear Behavior: Transfer Functions 25

6 BWR Nonlinear Behavior: Limit Cycles 35
- 6.1 Background 35
- 6.2 Reactivity Feedback During Limit Cycle Oscillations 35
- 6.3 Reactor Response to Sinusoidal Reactivity Perturbations 37
- 6.4 Physical Mechanism of the BWR Limit Cycle 39
- 6.5 The Average Power Increase 40
- 6.6 Limit Cycle Stability 40

7 Sensitivity to Physical Parameters 42
- 7.1. Parameters Affecting the Core-Wide Instability Mode 42
- 7.2. Parameters that Favor the Out-of-Phase Instability Mode 42

8. References 44

Appendix A Nomenclature 45

LIST OF FIGURES

Figure **Page**

Fig. 2.1. Example of a control system instability in a BWR5. 3
Fig. 2.2. Density wave mechanism introduces a time delay. 3
Fig. 2.3. Modes of oscillation for the coupled neutronic-thermohydraulic instability type 5
Fig. 2.4. Example of an in-phase oscillation event: LaSalle reactor, March 1988 6
Fig. 2.5. Example of average power range signal response to an out-of-phase instability. 7
Fig. 2.6. The axial mode of the neutronics is evident by the time delay observed between the oscillations at the LPRM A-level (bottom) and D-level (top) 7
Fig. 3.1. Illustration of the local pressure drop delay introduced by the density-wave mechanism 9
Fig. 3.2. Block diagram of the feedback paths for the coupled neutronics-thermohydraulics instability type . . . 10
Fig. 3.3. Typical reactor-power to fuel-surface-heat-flux transfer function in normalized units 11
Fig. 3.4. Typical transfer function from fuel surface heat flux to density reactivity coefficient in normalized units 12
Fig. 3.5. Flow patterns for the three main instability modes. 13
Fig. 3.6. Simplified block diagram of BWR dynamics showing the two main feedback paths 14
Fig. 4.1. Schematic diagram of the interface between thermohydraulics and neutronics for a typical BWR stability calculation using point kinetics 18
Fig. 4.2. Schematic diagram of the interface between thermohydraulics and neutronics for a typical BWR stability calculation using 1-D neutronics 20
Fig. 4.3. Schematic diagram of the interface between thermohydraulics and neutronics for a typical BWR stability calculation using 3-D neutronics. 21
Fig. 4.4. Schematic algorithm for the solution of BWR thermohydraulic problems with multiple channels 22
Fig. 5.1. Closed loop reactivity to power transfer function $(\%\Delta k/k)^{-1}$. Positive 180° phase shift at peak frequency indicates unstable conditions. 26
Fig. 5.2. Typical closed loop reactivity to power transfer function and observable features 26
Fig. 5.3. Root locus of a typical BWR reactivity to power transfer function 27
Fig. 5.4. Open-loop reactivity to power transfer function (unitless). 27
Fig. 5.5. Total feedback reactivity transfer function from power to reactivity ($\%\Delta k/k$), showing the contribution from density and Doppler feedbacks 28
Fig. 5.6. Individual channel power to density reactivity transfer function gain ($\%\Delta k/k$) for each thermohydraulic channel type. 29
Fig. 5.7. Individual channel power to density reactivity transfer function phase (deg) for each thermohydraulic channel type. 29
Fig. 5.8. Individual channel flow to density reactivity transfer function gain ($\%\Delta k/k$) for each thermohydraulic channel type. 31
Fig. 5.9. Individual channel flow to density reactivity transfer function phase (deg) for each thermohydraulic channel type. 31
Fig. 5.10. Core power to individual channel flow transfer function gain (normalized) for each thermohydraulic channel type. 32
Fig. 5.11. Core power to individual channel flow transfer function phase (deg) for each thermohydraulic channel type. 32
Fig. 6.1. Illustration of the development of a typical limit cycle in phase space 35
Fig. 6.2. Reactivity-to-power (G) and power-to-reactivity (H) transfer functions for a typical BWR 36
Fig. 6.3. Open-loop (GH) transfer function for a typical BWR 36
Fig. 6.4. Power response to sinusoidal reactivity with small bias 37
Fig. 6.5. Power response to sinusoidal reactivity with large bias 38
Fig. 6.6. Power response to sinusoidal reactivity with the right bias 38

LIST OF TABLES

Table **Page**

Table 5.1. Description of thermohydraulic regions used for the LaSalle simulation 25
Table 5.2. Gains of the individual channel power to density reactivity feedback transfer function at 0.4 Hz. Gains are normalized to the gain of the highest power channel. 30
Table 5.3. Effect of checker board pattern loading on core-wide decay ratio 33
Table 5.4. Sensitivity of calculated core-wide decay ratio to recirculation loop gain for a uniform and a skewed radial power distribution 33
Table 6.1. Calculated limit cycle parameters as a function of peak magnitude 39

1 Introduction

This report contains a review of issues related to density-wave instabilities in boiling water reactors (BWRs). The goal of this report is not to present new information; it is to collect information and ideas that are generally known and accepted in the field of BWR stability but have not been published in a coherent and concise style in any other document. The number of people working in the field of BWR stability has grown over the past years to a respecTable number (e.g., there were close to 100 participants in a recent BWR stability international workshop held at Brookhaven National Laboratory); nevertheless, the field is still small enough so that personal communication is an effective way of conveying information. This report is a summary of many such personal communications as well as formal oral presentations.

Section 2 of this report describes the types of instability modes expected in operating reactors. These modes are (1) the channel thermohydraulic instability mode, (2) the core-wide instability mode, and (3) the out-of-phase instability mode. Section 3 presents the physical mechanisms leading to each type of instability, and Sect. 4 summarizes some common mathematical models used in stability calculations. The main approximations used in these mathematical models are presented, and their impact on the accuracy of the calculations is reviewed. In Sect. 5, the linear behavior of a typical BWR is studied through the use of transfer functions, and Sect. 6 contains a study of the nonlinear behavior and limit cycle development. Section 7 presents a summary of the sensitivities to physical parameters.

2 Types of Instabilities Observed in BWRs

Boiling water reactors have complex dynamic responses that result in many instability types, and each of these types may have different modes of oscillation. This section describes the most common instability types and gives some examples of how they are manifested in commercial BWRs.

The names given to each of the instability types are not universal, and this causes confusion at times. It is not within the scope of this report to set a new nomenclature standard; therefore, we will use some of the synonyms most commonly used in the literature.

2.1 Control System Instabilities

Control system instability is the most common type of instability a reactor designer encounters. It is related to the action of controllers that, through actuators, attempt to regulate some of the variables of the reactor. BWRs are very complex nonlinear dynamic machines, which makes their control design difficult. For example, a controller that is optimized to respond at 100% flow might become unstable at 30% flow because of system nonlinearities. Also, improper maintenance might result in controller gain adjustments that cause unstable operation at different operating conditions.

This type of instability usually manifests itself as low-frequency oscillations (BWR controllers are typically slow) in either feedwater flow, feedwater temperature, or reactor pressure. These oscillations are caused by the action of an actuator (typically a valve) that follows the signals given by the control system. Most of the time, the unstable control action is so small (and the reactor so forgiving) that these instabilities go unnoticed. They result in low-frequency power or flow oscillations (of the order of 3 to 5%), which are practically masked by the normal reactor noise. Nevertheless, these instabilities should be detected and corrected, if for no other reason than to avoid excessive wear of the control actuators that may cause a more serious problem later on.

There are two main controllers that affect the core of a BWR: the pressure controller and the reactor water level controller. The reactor power is, typically, not controlled automatically, and it is set manually by the operator through the positioning of control rods and recirculation pump speed. The most complex of the BWR controllers is the level control caused by "non-minimum-phase" effects, the "shrink-and-swell" phenomenon, and the effect on power of the core inlet flow subcooling. To solve this problem, the designers opted for the so-called "three-element" controller that not only takes into account the reactor water level but also the feedwater and steam flows. This results in a control design that is fairly sensitive to feedback gains and changes in operating conditions.

Several control-system-type instabilities have been reported. For example, Fig. 2.1 shows a sinusoidal oscillation observed in the core inlet flow of a BWR5 when it was operated at minimum recirculation pump speed (60% power, 46 Mlb/h).[1] The observed oscillation is quite small in magnitude (±0.5 Mlb/h or about 1% of current flow) and its period is of the order of 50 s, so that this type of oscillation can easily go unnoticed in the control room.

2.2 Channel Thermohydraulic Instabilities

Heated channels under two-phase flow regime are susceptible to a variety of instability types. Lahey[2] classifies these instabilities into two broad categories: static and dynamic. The static instabilities are explained in terms of steady-state laws, whereas dynamic instabilities require the use of dynamic conservation equations.

Examples of static instabilities[2] are (1) flow excursion or Ledinegg instability, (2) flow regime "relaxation" instability, and (3) geysering or chugging. All of these instability types have in common the existence of two equilibrium points, and the system tends to "jump" from one to the other. Examples of dynamic instabilities[2] are (1) density-wave oscillations, (2) pressure drop oscillations, and (3) flow regime induced instabilities.

The most common instability for commercial BWRs is the density-wave instability, which is also referred to as the channel flow instability. This type of instability can be described as follows: given a flow perturbation, a "wave" of voids travels upward through

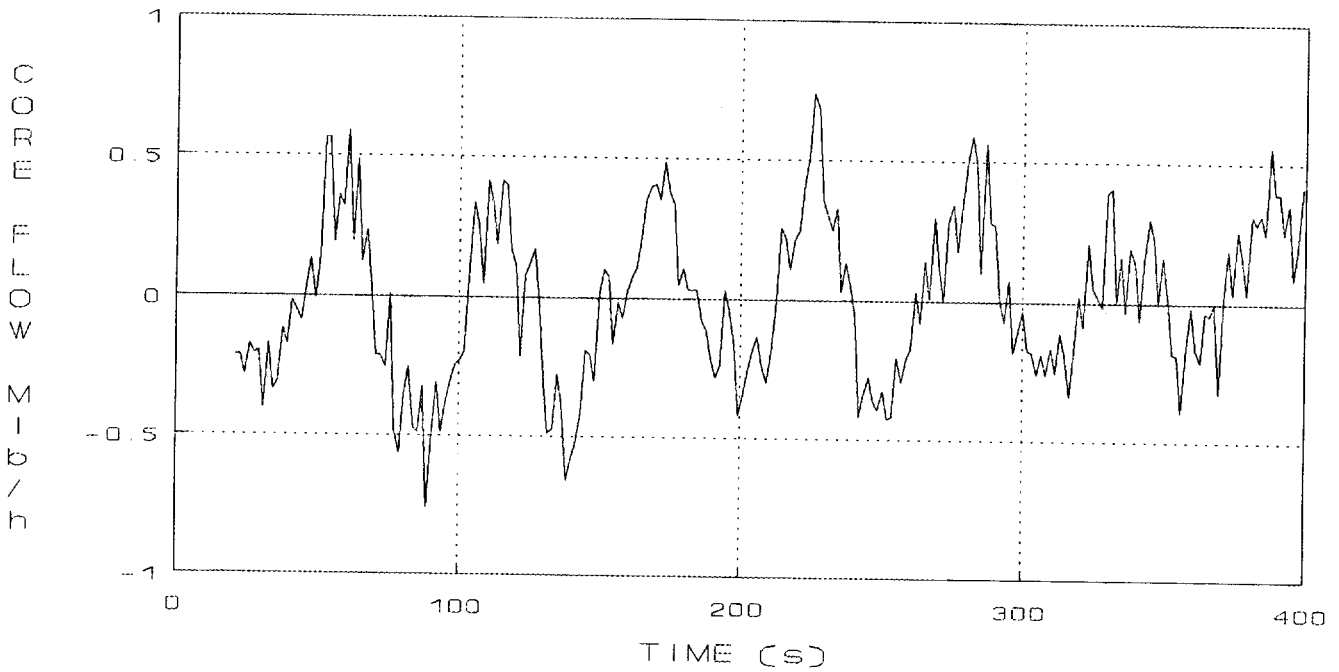

Fig. 2.1. Example of a control system instability in a BWR5.

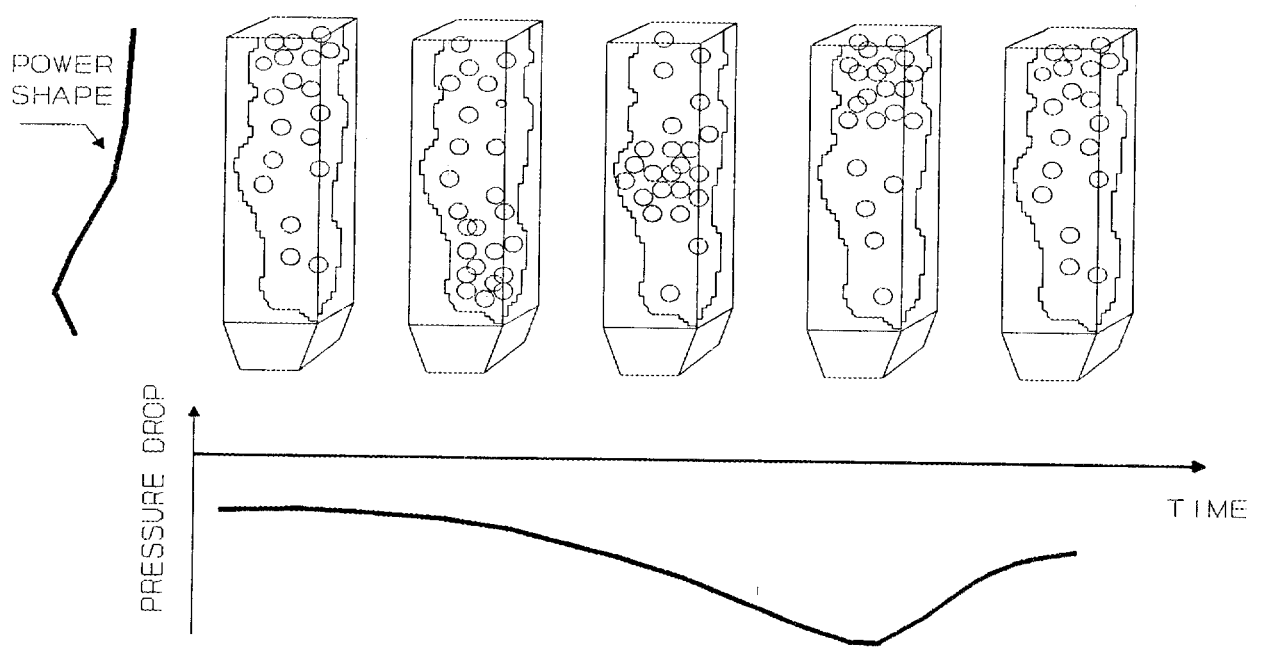

Fig. 2.2. Density wave mechanism introduces a time delay. The effect of a power pulse is seen up to 2 seconds later in the channel pressure drop due to void propagation delay

the channel producing a pressure drop that is delayed with respect to the original perturbation (Fig. 2.2). An increase in flow typically induces an increase in pressure drop and a negative feedback that tends to reduce the flow perturbation. The density-wave phenomenon, however, delays this feedback, and, at some frequency, the delay is equivalent to a 180° phase lag; thus, at this frequency, the pressure drop feedback is positive. If the gain is large enough, the channel flow becomes unstable and oscillates at that frequency.

The two main modes of oscillation that exist for the channel thermohydraulic instability are single-channel and parallel-channel instabilities. In the parallel-channel mode of oscillation, the flow in one channel increases while the flow in the other channel decreases; thus, this mode of oscillation is called out-of-phase flow instability. During out-of-phase oscillations, the channel void fraction follows trends opposite to those of the flow, so that the pressure drop is the same across both channels. Experiments and analytical studies show that the parallel-channel mode of flow oscillation dominates the single-channel mode.[2] This is caused by the increased inlet flow feedback that is imposed by the constant-pressure-drop boundary condition (see Section 3.3).

Another mode of density-wave flow instability that has been observed in experiments is the three-channel type of instability. In this mode three channels (or groups of channels) oscillate 120° out-of-phase with respect to each other. The void fractions oscillate opposite to the local channel flow, and, as was the case with two-parallel-channel oscillations, the pressure drop is maintained constant across all the oscillating channels.

Channel thermohydraulic oscillations are also called "local" instabilities because they may affect a single channel in the core of a large BWR that has up to 800 channels. This type of instability, should it occur, is quite dangerous and it may go undetected for a long period of time because it only affects the local flow of a single channel. The local void oscillations will be seen in the local power range monitors (LPRMs) but will probably be hard to distinguish in the average power range monitors (APRMs) time traces. The reactor only takes protective action (i.e., scram) based on APRM signals. Local flow oscillations of significant amplitude have the potential for causing transition boiling and prolonged periods of dryout condition, which can lead to fuel clad failure, if fuel surface rewetting is prevented by the film boiling.

The only reported case of channel thermohydraulic instability occurred in the Garigliano reactor in Italy in the mid-1960s during special tests. A special turbine flowmeter was installed at the outlet of some channels in this reactor. One of the flowmeters failed in a locked position, which caused a significant increase in the two-phase pressure drop of that channel. This caused the channel flow to become unstable, and it oscillated following a single-channel mode of instability.

2.3 Coupled Neutronic-Thermohydraulic Instabilities

The dominant type of instabilities in commercial BWRs is the coupled neutronic-thermohydraulic instability, and approximately 20 events attributed to this type of instability have been reported worldwide. Although most of these instabilities were produced during special stability tests, some of them occurred during normal operation and caused the reactor to scram.

The coupled neutronic-thermohydraulic type of instability is also called the reactivity instability because it involves the changes in reactivity caused by void fraction fluctuations. Because of the density-wave effect, the reactivity feedback caused by changes in void fraction is delayed as the voids travel upward through the channel. If the delay is long enough or the void feedback coefficient is strong enough, the reactor configuration is unstable, and the neutron flux oscillates with a frequency close to the inverse of the density-wave time constant (i.e, the time delay caused by the voids traveling through the core).

This instability type is called coupled neutronic-thermohydraulic because it involves two feedback loops: (1) the neutronic feedback described above and (2) the thermohydraulic feedback that affects the inlet flow rate in a manner similar to that of the channel flow stability. This is the dominant mode of instability

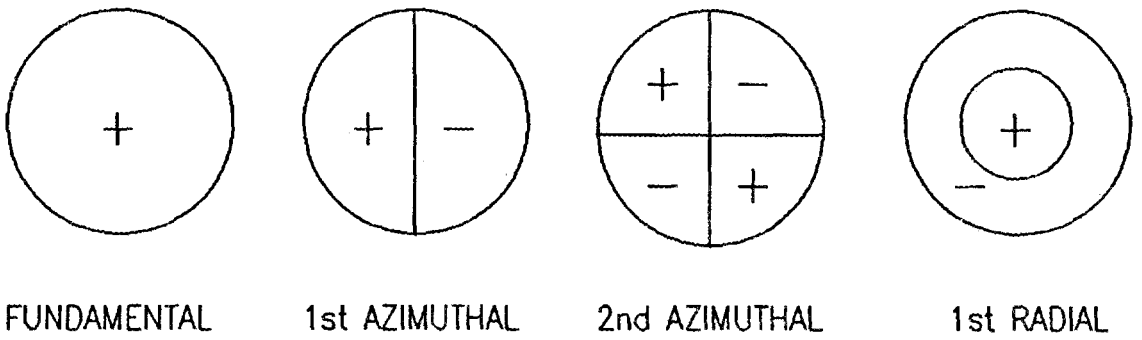

Fig. 2.3. Modes of oscillation for the coupled neutronic-thermohydraulic instability type

in BWRs because it adds all the destabilizing effects of the thermohydraulic feedback to those of the neutronic feedback.

The two modes of oscillation that are commonly recognized for this type of instability are the core-wide or in-phase mode and the regional or out-of-phase mode. In the core-wide mode, the power and inlet flow of the whole core oscillate in phase for all channels. In the out-of-phase mode that has been observed in experiments and instability events worldwide, the power of half of the core oscillates out-of-phase with respect to the power of the other core half. The inlet flows of both halves of the core are also out-of-phase with respect to each other.

The different modes of the reactivity-type of instability have been explained based on the spatial modes of the neutron flux field that are coupled to the thermohydraulic reactivity feedback. The neutron flux caused by a spatial distribution of reactivity tends to organize itself in the form of its dominant modes (i.e., harmonics) in a manner similar to that of a string that oscillates with different harmonics (i.e., modes) depending on the initial condition chosen. Figure 2.3 shows the dominant modes of the neutron field in the radial direction for a cylindrically shaped reactor. Depending on the type of excitation and the particular reactor conditions, one mode dominates the other. This hierarchy of modes and how and when the out-of-phase mode dominates the fundamental core-wide mode are discussed in Sect. 3.

Because of their spatial distribution, core-wide oscillations are readily observed and measured with the reactor's APRM instrumentation. In this manner, large core-wide oscillations result in an automatic scram when the plant protection system setpoint is reached. Out-of-phase oscillations, however, are not readily detectable by the APRM system because the oscillations in one side of the reactor cancel the ones in the other side. Indeed, a perfectly symmetric out-of-phase oscillation and LPRM distribution would result in no perceived oscillation in the APRM signal. Fortunately, the real world oscillations are not perfectly symmetric with respect to the LPRM distributions of detectors, and nonlinearities in the neutron flux response make perfect cancellation impossible. Nevertheless, attenuation factors of 7 to 10 have been observed in experiments.[3] This implies that by the time the APRM oscillation reaches the 120% safety setpoint, local LPRM oscillations might be as high as 1200%. Thus, at the present time, out-of-phase oscillations pose a dangerous threat to the integrity of present reactors that do not have automatic protection against these oscillations. Utilities in the United States are currently required to scram manually upon the detection of any type of oscillation,[4] based mostly on LPRM upscale and downscale alarms, which are sensitive to large out-of-

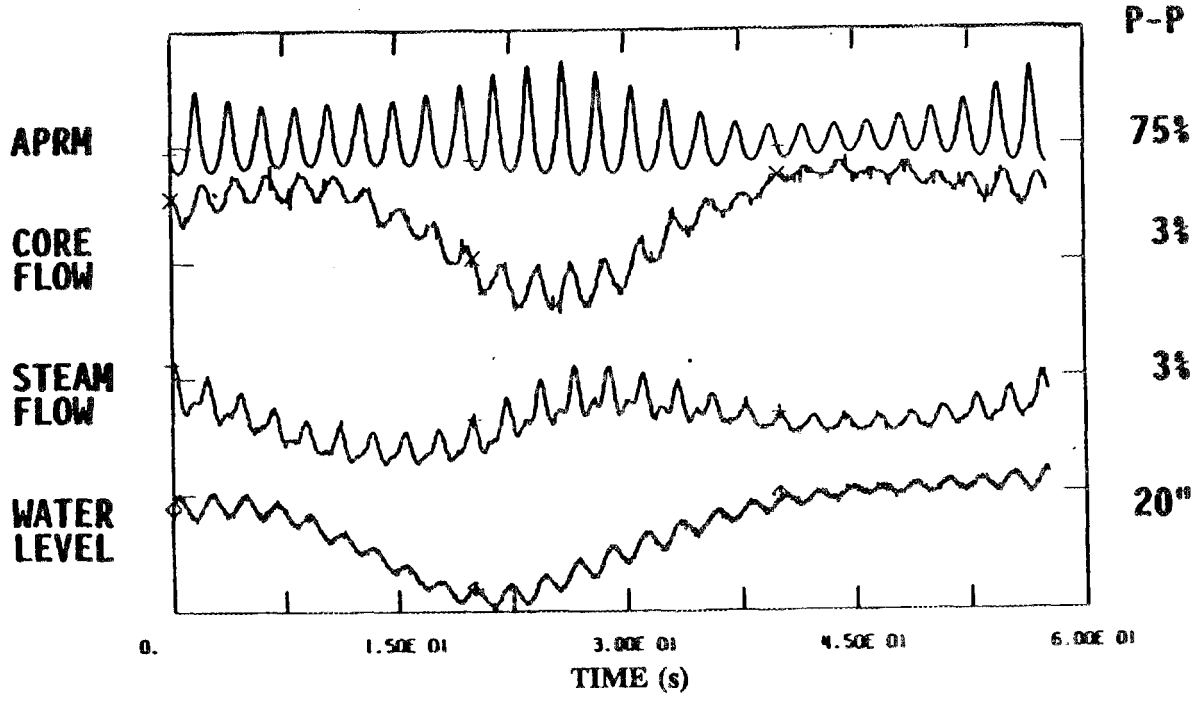

Fig. 2.4. Example of an in-phase oscillation event: LaSalle reactor, March 1988

phase oscillations. An automatic protection system for all types of expected modes of oscillation is currently being designed by U.S. utilities and should be implemented in the near future.

Figures 2.4 and 2.5 show an example of in-phase and out-of-phase instability events in commercial BWRs. The oscillation in the LaSalle reactor (Fig. 2.4) resulted in an automatic scram within a minute from the end of this time trace due to high APRM flux (< 118%). The oscillation event in the Ringhals BWR (Fig. 2.5) was in the out-of-phase mode and was terminated by a partial scram performed manually by the operator. The LaSalle event was compounded by a partial failure of a feedwater heater controller valve that was sticking open until the controller demand was large enough to force it to close all the way. This was the cause for the modulation in the limit cycle amplitude observed in Fig. 2.4. Thus, the LaSalle event is also an example of a control system instability that drives a low-frequency power oscillation.

There is some evidence, not yet completely understood, that axial modes play an important role in oscillations caused by the coupled neutronic-thermohydraulic instability type. For instance, Fig. 2.6 shows the time delay between the oscillations at different LPRM levels during an in-phase core-wide oscillation. It is well known that the static modes of systems with distributed spatial feedback are not necessarily orthogonal to each other. Thus, the fundamental mode may excite the first axial mode by the propagation of voids through the density-wave mechanism, and vice versa. This is an area that deserves more research effort, especially in the study of implications to the applicability of codes based on the point kinetic approximation, which only models the fundamental neutronic mode.

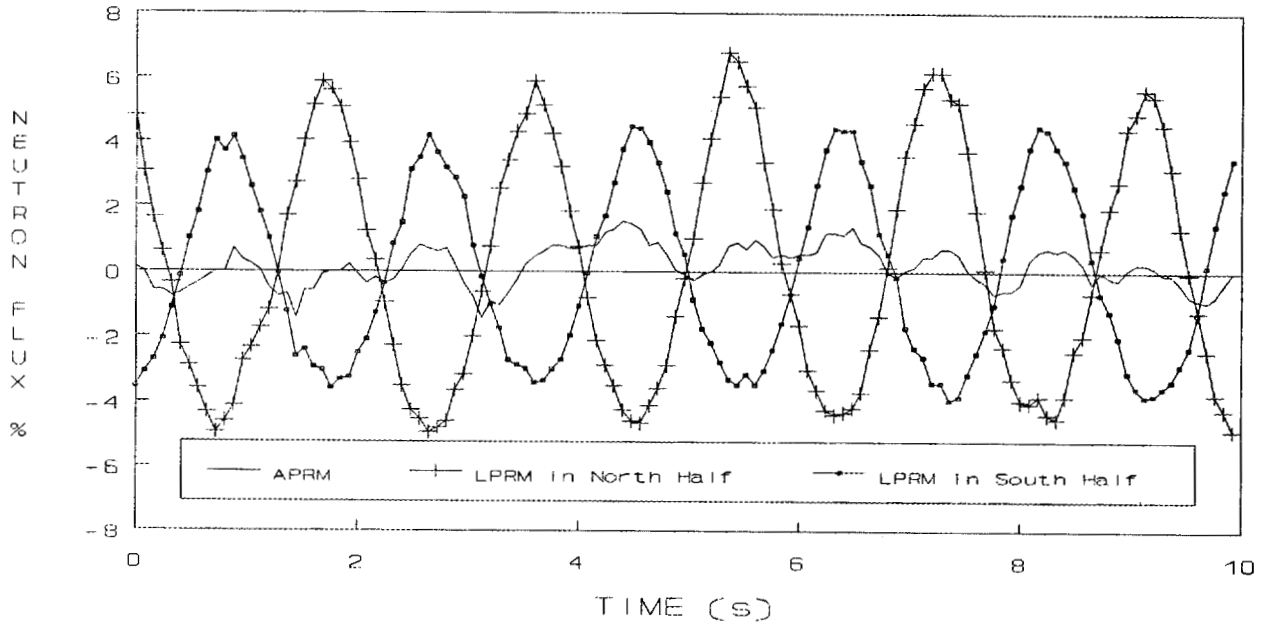

Fig. 2.5. Example of average power range signal response to an out-of-phase instability. Note the double frequency (1 Hz) caused by the slight asymmetry in the oscillation

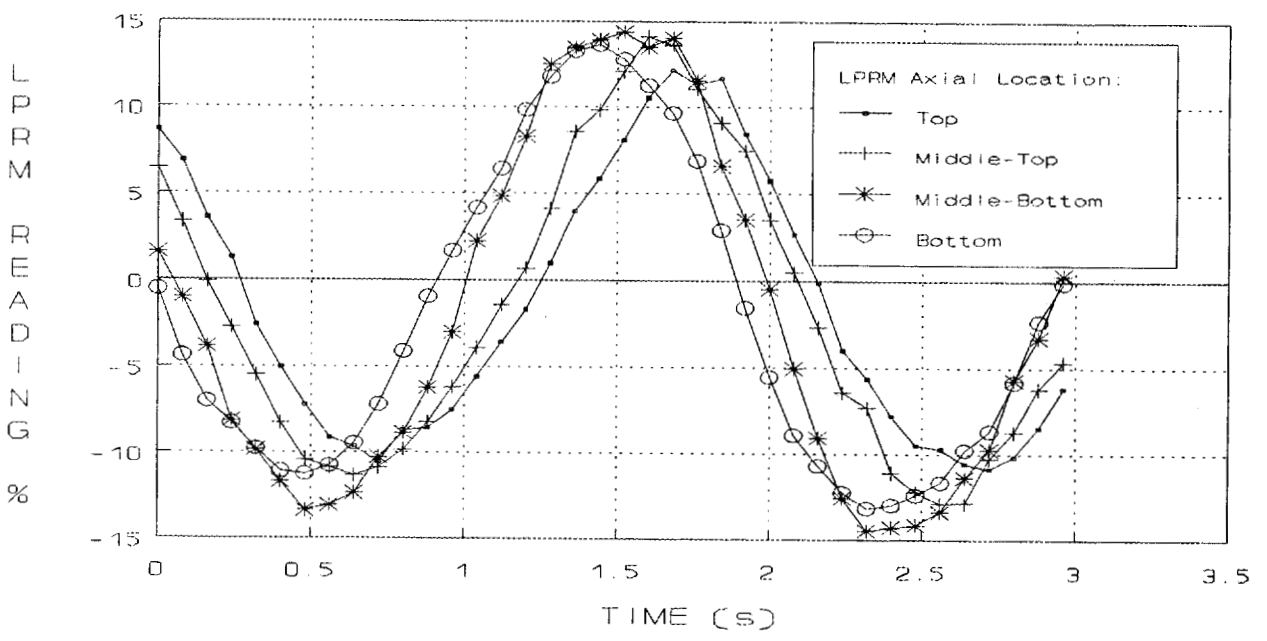

Fig. 2.6. The axial mode of the neutronics is evident by the time delay observed between the oscillations at the LPRM A-level (bottom) and D-level (top)

3 Physical Mechanisms Leading to Instabilities in BWRs

This section describes the physical mechanisms that lead to the observed instabilities in BWRs. As stated in Sect. 2, the most probable instabilities in BWRs are either the channel flow instability or the coupled neutronic-thermohydraulic instability. Both of these types of instabilities have their roots in the density-wave mechanism, which adds a significant delay to the feedback path. Thus, this section describes first the density-wave mechanism, which governs the inlet flow feedback, and later the neutronic feedback, which determines the power level.

3.1 The Density-Wave: Flow Oscillations

The density wave causes a delay in the local pressure drop that is caused by a change in inlet flow. Because of this delay, the sum of all local pressure drops may result in a total drop that is out-of-phase with the inlet flow. The basic mechanism causing flow instabilities in BWRs is the density wave, whose effect on pressure drop is illustrated in Fig. 3.1. The coolant in commercial BWRs flows upward through the core and is guided by bundle boxes that surround a matrix of fuel pins (typically an array of 8 by 8 or 9 by 9 pins). Thus, variations in density in the bottom part of the channel travel upward with the flow. For example, if the inlet flow is decreased while the channel power is kept constant, there is an increase in the number of voids in the channel that will travel upward as a packet forming a propagating density wave. This packet of voids produces a change in the local pressure drop at each axial location, which is delayed axially by the density-wave propagation time (i.e., the effective time for the voids to move upward through the core). In two-phase flow regimes, the local pressure drop is very sensitive to the local void fraction and is very large at the outlet of the channel where the void fraction is greatest; thus, a significant part of the pressure drop is delayed with respect to the original perturbation.

If the inlet flow is perturbed sinusoidally, the local pressure drops are also sinusoidal (within the linear range), but they are delayed with respect to the perturbation (Fig. 3.1). The total pressure drop across the channel is the sum of a series of delayed sinusoids (the local pressure drop) and, thus, also has a sinusoidal form that is delayed with respect to the flow perturbation. If the channel outlet pressure drop (the one that is more delayed) is larger than the inlet pressure drop, the total pressure drop may be delayed 180° with respect to the inlet flow and, therefore, have the opposite sign. This is the case in Fig. 3.1, where an increase in inlet flow results in a decrease in channel pressure drop. One might think that this channel behaves as if it had a "negative" effective friction coefficient at this particular frequency; thus, the channel flow is unstable, and any inlet flow perturbation feeds on itself (positive feedback), and oscillations grow at that unstable frequency. The critical point at which the channel flow instability starts is when the outlet (i.e., delayed) local pressure drop equals the pressure drop at the inlet at a particular frequency. In this case, we have a channel with an effective zero friction at that frequency, so that any perturbation sustains itself.

In the above description we have simplified the argument by talking only about an inlet pressure drop (which is also called the single-phase pressure drop) and an outlet, or delayed, pressure drop (which is also called the two-phase pressure drop). In reality, as illustrated in Fig. 3.1, the local pressure drop is a continuous function of axial position and the situation has to be modelled accurately. However, it sometimes helps to have a simplified mental picture (like the one presented above) in which all the issues are black or white and therefore easier to understand. This is the simple view that will be used for arguments throughout this paper, the reader should understand that the real physical problem is more complex, and that a simple mental model, although helpful, is not a substitute for a detailed numerical calculation.

The relative flow stability of a channel depends on the amount of inlet flow feedback, and the inlet flow feedback is a function of the channel boundary conditions. The three main types of boundary conditions are (1) constant pressure drop, (2) variable pressure drop, and (3) constant inlet flow.

A constant-pressure-drop boundary condition may be achieved in a test stand by having a large bypass flow in parallel with the test channel. If a single channel were to become unstable in a BWR that is

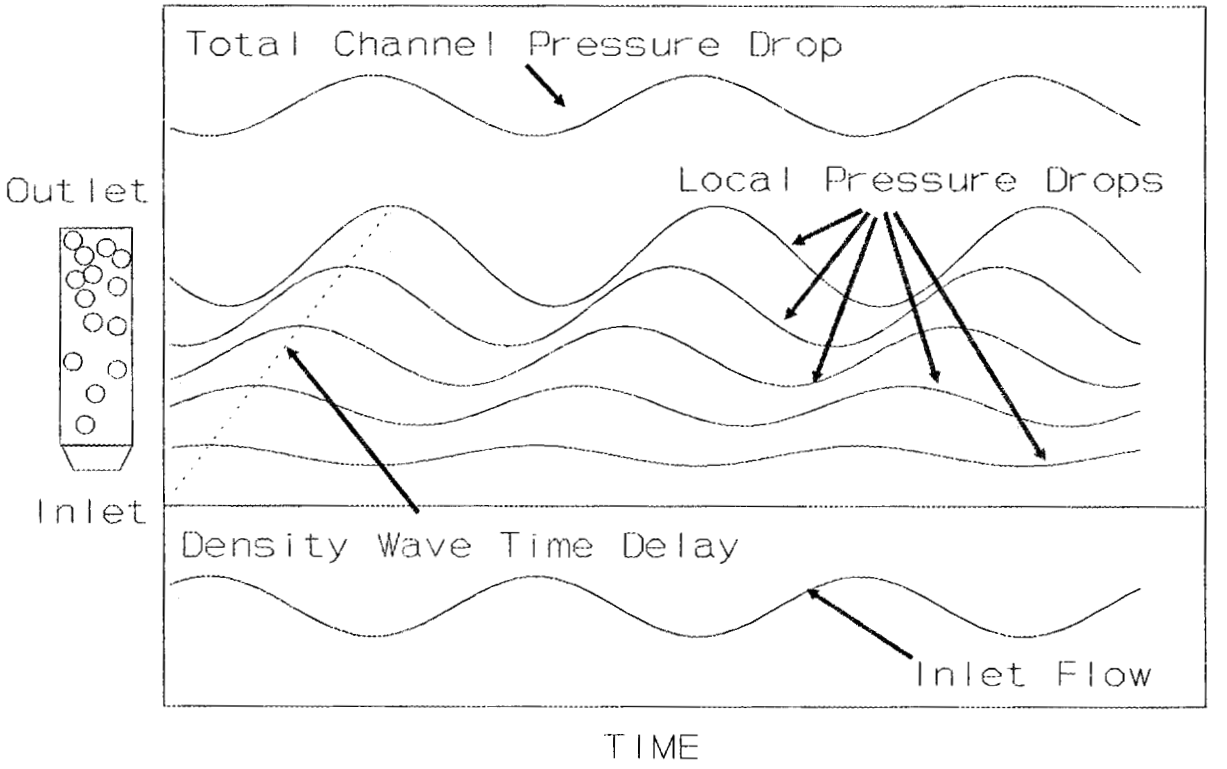

Fig. 3.1. Illustration of the local pressure drop delay introduced by the density-wave mechanism

formed of as many as 800 bundles, the boundary condition would be forced by the remaining 799 bundles, and it would remain essentially constant across the unstable channel. This type of boundary condition is the most unstable of the three because it results in the largest number of inlet flow feedback oscillations required to maintain the constant pressure drop.

A variable pressure drop boundary condition occurs when the channel inlet flow is determined by the recirculation loop and pump dynamics. In this case, the channel pressure drop at a particular flow and time must match the pressure drop across the recirculation loop plus the pressure gain at the pump for the particular loop flow. For this pressure balance, dynamic terms, such as inertia, have to be taken into account in the channel as well as in the circulation loop. Because the pressure drop across the channel is allowed to oscillate according to the recirculation-loop dynamics, the inlet flow feedback is not as strong in this case as in the constant-pressure-drop boundary condition.

A constant inlet flow boundary condition can be achieved in a test stand by having a constant displacement pump feed the channel a constant inlet flow regardless of pressure. This is the most sTable boundary condition. Indeed, because the flow is constant, it cannot oscillate; therefore the channel is always stable.

The physical processes that cause flow oscillations are hard to visualize, but they are slightly easier for the case of the constant-pressure-drop boundary condition. Let us assume an unstable channel that, as

described before, has an effective negative friction coefficient at a frequency. Let us further assume that the pressure drop across this channel is maintained constant by (for instance) maintaining a large flow through a bypass region in parallel with the channel. Then, if a perturbation occurs that increases the inlet flow, the negative effective friction coefficient would tend to decrease the pressure drop. To compensate and keep the pressure drop constant, the channel increases the inlet flow even further, which causes a runaway instability. What complicates the situation is the fact that the effective friction coefficient is only negative at a particular frequency; thus, the flow increase is not an average flow increase but a flow increase at the frequency. In other words, the instability results in an oscillation of that frequency with an exponentially growing amplitude. Nonlinearities in the system eventually cancel the growth of the oscillation, and a limit cycle is established at a finite oscillation amplitude.

3.2 Neutronic Feedback During Oscillations

In the previous section, we described the density wave in relation to flow instabilities. For those instabilities, only flow is involved, and the power generation term in the fuel is assumed constant. In BWRs, the power generation is directly related to the neutron flux, which is a function of the reactivity feedback and, therefore, depends strongly on the core average void fraction. Thus, when a void fraction oscillation is established in a BWR, the power oscillates according to the neutronic feedback.

The neutronic feedback path is different from the inlet flow feedback path. The neutronic feedback involves (1) the neutron dynamics, which determine the power generated in the fuel; (2) the fuel dynamics, which define the heat flux from fuel to coolant; (3) the channel thermal hydraulics, which characterize the void fraction response to changes in heat flux and include the inlet flow feedback through the recirculation loop; and (4) the reactivity feedback

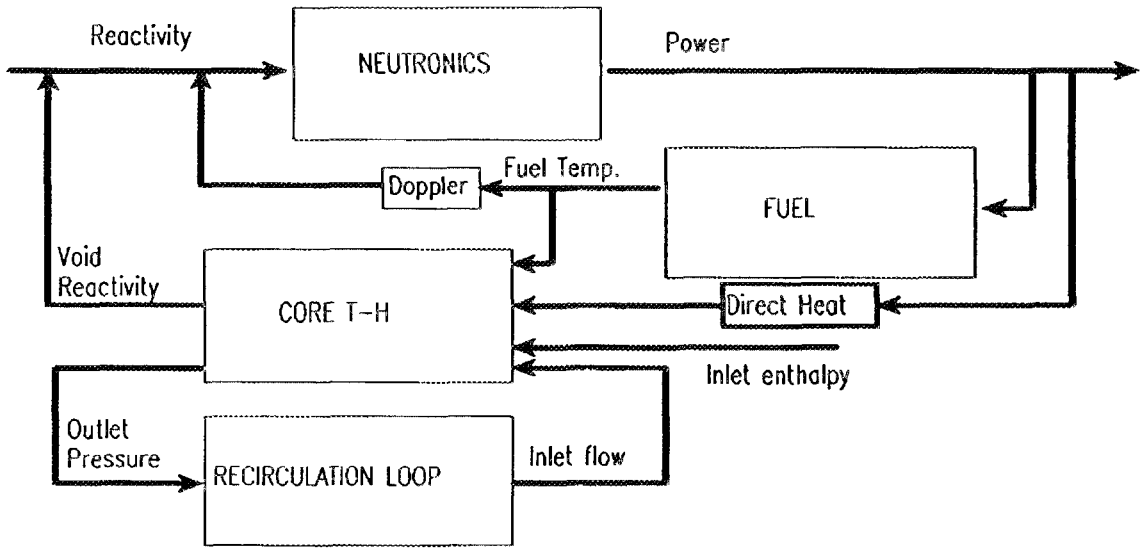

Fig. 3.2. Block diagram of the feedback paths for the coupled neutronics-thermohydraulics instability type

dynamics, which relate the void fraction distribution to a reactivity value that affects the neutron dynamics. These feedback paths are illustrated graphically in Fig. 3.2. One important difference between the neutronic feedback and the flow feedback paths is caused by the fuel transfer function. Before the power generated by the neutronics can feed back through the moderator density, it has to change the fuel temperature to alter the heat flux from fuel to coolant. The fuel in commercial BWRs responds relatively slowly with a time constant between 6 s and 10 s. This results in a single pole break frequency of the order of 0.03 Hz. Since the unstable oscillations occur approximately one decade above this break frequency (i.e., at approximately 0.3 to 0.5 Hz), the fuel adds almost a 90° phase delay to the feedback. Furthermore, the gain of the fuel transfer function decreases inversely proportional to the frequency for frequencies between 0.1 and 1.0 Hz. This effect can be seen in Fig. 3.3, which shows a typical power-to-heat-flux transfer function calculated by the LAPUR[5] code. Thus, the fuel has some destabilizing effect because of its phase delay, but it also has a significant stabilizing effect caused by its inherent filtering of the oscillation amplitude at frequencies higher that 0.1 Hz. Changes in fuel time constant affect the reactor stability in two ways, but experience has shown that the gain effect is dominant over the phase effect. Thus, decreasing the time response of the fuel (i.e., smaller diameter fuels or increased pellet-clad gap conductance) has a destabilizing effect in general.

The void reactivity feedback is computed by performing a spatial averaging of the void distribution in the core weighted by the local void reactivity coefficients and the local neutron flux and adjoint. In mathematical terms, the reactivity feedback, $\Delta\rho$, due to a void perturbation, $\Delta\alpha$, can be written as shown in Eq. (3-1),

$$\Delta\rho(t) = \int_0^H \int_0^R \Phi^+(r,z)\ \Phi(r,z) \left(\frac{d\rho}{d\alpha}\right)(r,z)\ \Delta\alpha(r,z,t)\,dr\,dz \tag{3-1}$$

where Φ and Φ^+ are the normalized neutron flux and its adjoint, respectively, and $d\rho/d\alpha$ is the local density reactivity coefficient.

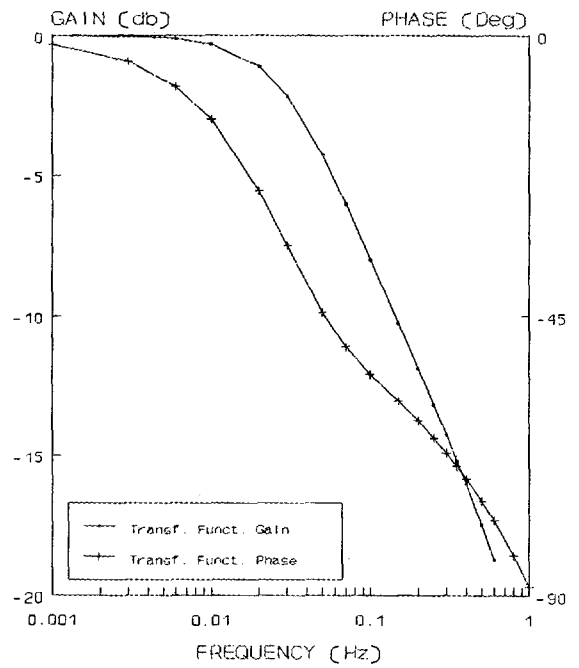

Fig. 3.3. Typical reactor-power to fuel-surface-heat-flux transfer function in normalized units

The averaging described by Eq. (3-1) results in a phase delay of slightly over 90 and a large filtering effect (i.e., gain reduction) for frequencies higher than the inverse of the density-wave time constant. Figure 3.4 illustrates this effect in the LAPUR-calculated transfer function from fuel surface heat flux to density reactivity feedback. The units in this figure are normalized to the average (i.e., zero frequency) value because only the shape of the transfer function is relevant to this general discussion. The absolute gain value of this transfer function will depend on the particular characteristics of the reactor being modeled; for example, the gain is directly proportional to the density reactivity coefficient. The filtering effect on the channel gain is very significant at high frequencies (Fig. 3.4), and it results in a fast roll-off that, for all practical purposes, eliminates all frequencies higher than the fundamental oscillation frequency from the feedback path. This is the reason for the observation that in time domain codes the reactivity feedback is essentially sinusoidal even under large limit cycle

conditions when the neutron flux has a significant amount of higher harmonic contamination. The filtering effect observed above is caused by the spatial averaging introduced by Eq. (3-1) combined with the density-wave mechanism. For example, if the reactor power (and, consequently, the fuel heat flux) is oscillated at a high frequency, there will be an associated density wave formed by the void perturbations that will travel upward through the channel. If the oscillation frequency is higher than the density-wave characteristic time delay, the wave front will not have time to leave the top of the channel before the next wave front is created. In this manner, when the average void fraction is calculated using Eq. (3-1), the positive and negative parts of the wave cancel each other, and there is a significant decrease in overall density reactivity feedback. On the other hand, if the power oscillation is of a very low-frequency, the spatial averaging does not produce the canceling effect described above, and the gain is not reduced.

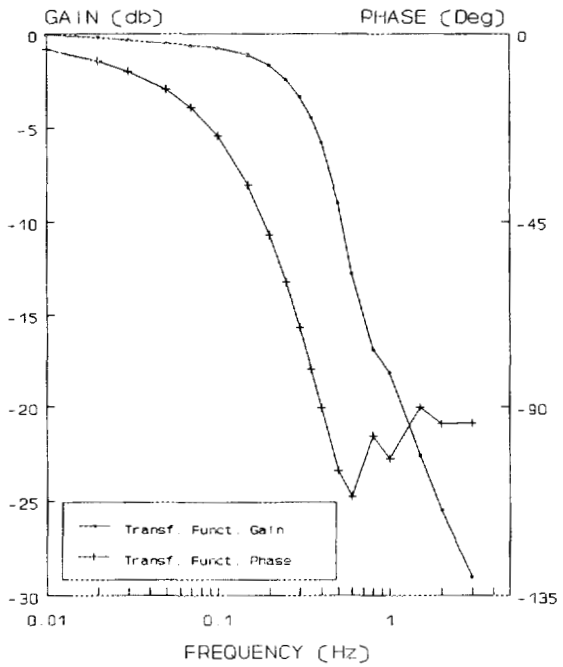

Fig. 3.4. Typical transfer function from fuel surface heat flux to density reactivity coefficient in normalized units

3.3 Boundary Conditions for Different Oscillation Modes

It has been established experimentally[6] that momentum dynamics and the recirculation-loop flow path play an important role in defining reactor stability because, for the fundamental mode of oscillation, any change in power is accompanied by a change in inlet flow. The amount of this change is determined by momentum dynamics in the core and recirculation-loop characteristics. However, an out-of-phase mode of oscillation in parallel channels does not require changes in total inlet flow because the two oscillating core regions adjust their flows to maintain equal pressure drops across the core. In other words, if the flow increases in channel 1, the flow of channel 2 decreases by the same amount (at least within the linear operating region), and the total flow remains unchanged. This mechanism allows for large flow oscillations within each channel, and it has the effect of increasing the gain of the thermohydraulic component in the BWR dynamics feedback, thus decreasing the reactor stability.

The mechanism described above is represented schematically in Fig. 3.5. In this figure, the arrows represent the flow intensity through the representative channels during an oscillation of period T. For the fundamental (core-wide) mode of oscillation, the whole core behaves as a unit, and the total core inlet flow oscillates in phase with the core pressure drop. In the out-of-phase mode of oscillation, a constant total core inlet flow is maintained by readjusting individual channel flows, and the core pressure drop is maintained constant. This flow pattern is graphically represented in Fig. 3.5 by two flow components: the in-phase component that remains constant, and the out-of-phase component that oscillates; the actual flow is the sum of the two components. When a single channel instability occurs, the inlet flow of the single unstable channel oscillates, but the total core flow and core pressure drop remains essentially constant because it is controlled by the large number of stable channels.

Thus, the boundary conditions that must be used to model the three instability modes are as follows:

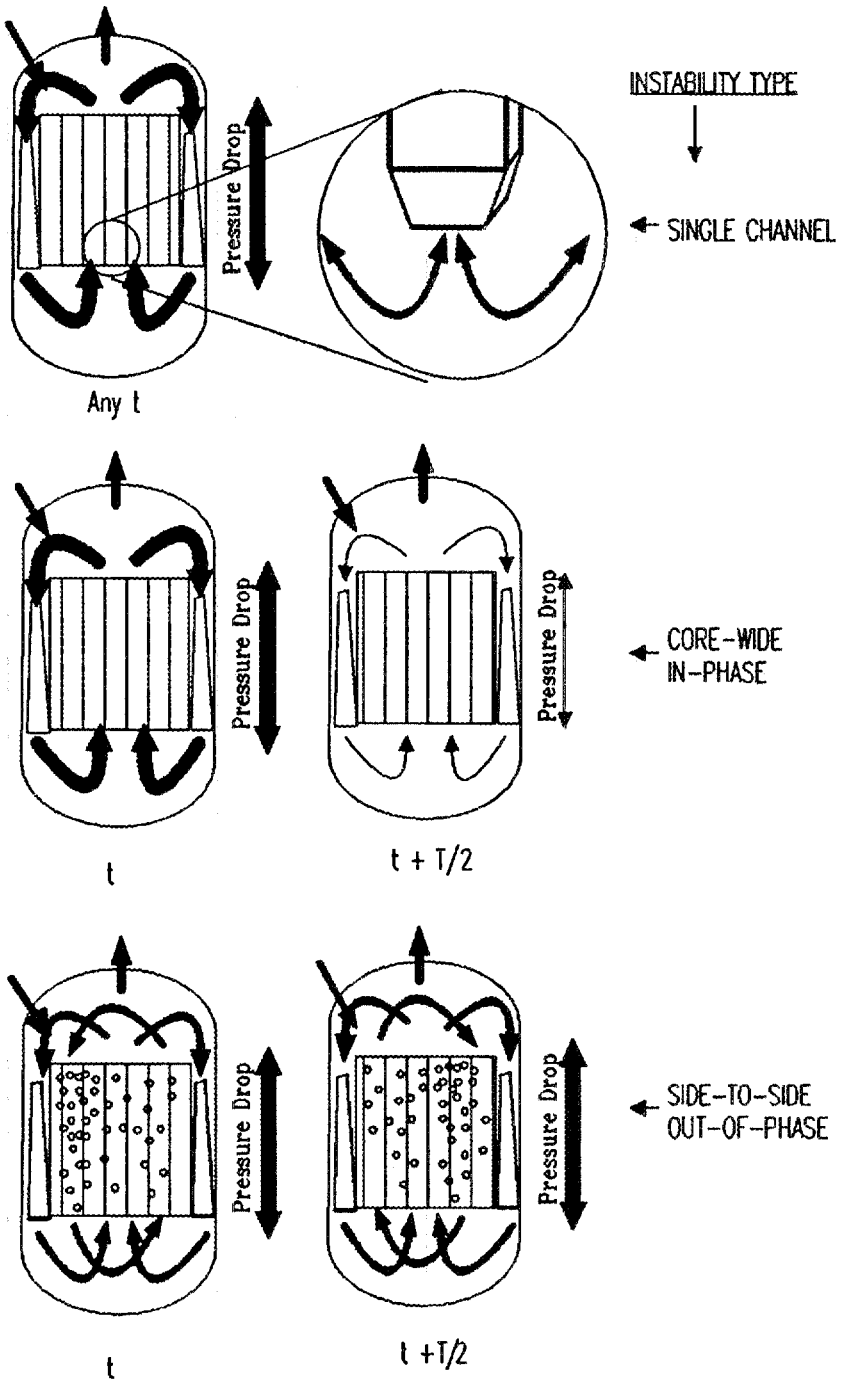

Fig. 3.5. Flow patterns for the three main instability modes. Arrow thickness indicates flow intensity. Arrow to the right of vessel illustrates core pressure drop

- Core-wide instability mode - variable pressure drop across the core that is determined by the recirculation-loop dynamics,
- Out-of-phase instability mode - constant pressure drop across all channels in the core, and
- Channel thermohydraulic instability mode - constant pressure drop across the channel.

A thermohydraulic model of a BWR includes fuel, core coolant, and recirculation-loop dynamics. The dynamic processes solved by most BWR stability codes can be summarized as follows: an energy balance in the fuel region yields the heat transferred to the core coolant. The energy and continuity balance equations are solved in the coolant region to obtain the core enthalpy (i.e., void fraction) distribution. Neglecting second-order effects, the momentum equation can integrate this distribution to yield the core pressure drop. The recirculation-loop momentum equation yields the core inlet flow from the pressure drop across the jet pumps, which must equal the pressure drop across the core. The thermohydraulic loop is closed when the inlet flow is coupled to the coolant energy and continuity equations. Finally, the thermohydraulic and neutronic models are coupled via the fuel temperature and void reactivity feedbacks, which yield the $\Delta\alpha$ term in Eq. (3-1). Thus, the two main feedback paths in the closed-loop dynamics of a BWR are (1) the inlet flow feedback, characterized by the reactor and recirculation-loop momentum dynamics, and (2) the neutronic feedback, caused by the void reactivity coefficient. These feedback paths are represented in Fig. 3.6.

In physical terms, the dominance of the out-of-phase and core-wide modes of unstable oscillations depends on the relative gains of the two feedback paths in Fig. 3.6. The out-of-phase instability mode has a very large gain for the inlet flow feedback (in essence the flow can oscillate as much as it wants without having to pay any friction "penalty" in the recirculation loop), but it has low gain from neutronic feedback because it corresponds to a damped subcritical mode. For the core-wide instability mode, the situation is reversed; the neutronic feedback is

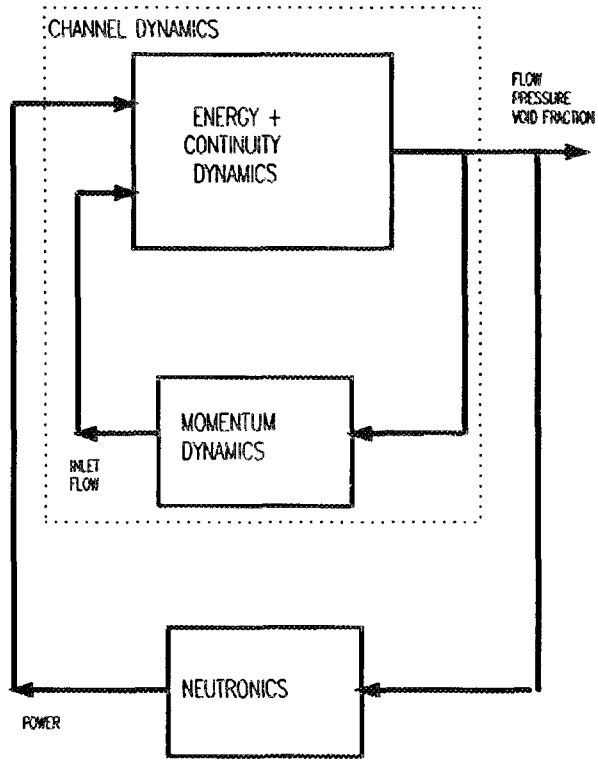

Fig. 3.6. Simplified block diagram of BWR dynamics showing the two main feedback paths

large, but the inlet flow feedback is smaller because flow oscillations are damped by the friction in the recirculation loop. Thus, either of the two instability modes (out-of-phase or core-wide) may dominate the response of the reactor. Which of the two will dominate depends on specific values of parameters as they affect the relative gain of the two main feedback paths.

The thermohydraulic equations in a particular channel are essentially the same for the out-of-phase mode as for the core-wide (fundamental) mode; they are based on the momentum, energy, and continuity equations. The only difference between the two modes arises on the core boundary conditions (i.e., inlet flow and pressure drop). For the core-wide mode, the boundary conditions are determined by the recirculation-loop dynamics. For the out-of-phase mode, however, the boundary conditions are fixed, and

they determine the necessary inlet flow to maintain a constant pressure drop across the core. This is a well-known boundary condition for parallel-channel oscillations and is caused by the common plena connecting all channels.

In frequency domain linear codes, the constant-pressure-drop boundary condition can be implemented either by properly connecting the individual open-loop transfer functions as they are combined to form the closed-loop or by setting the gain of the recirculation-loop pressure-to-flow transfer function to an arbitrarily large number and using an existing core-wide stability code. Both methods yield the same result because both minimize pressure drop variations.

In summary, there are two competing effects in the out-of-phase mode: on the one hand, the neutronics component is subcritical and tends to damp out oscillations; on the other hand, the thermohydraulic component in the out-of-phase mode has more gain than in the fundamental mode and tends to destabilize it. The relative importance of the two above effects depends on the degree of subcriticality of the out-of-phase mode. Thus, it seems plausible that there is a threshold subcritical reactivity at which the out-of-phase mode can become unstable, even if the fundamental mode is stable.

4 Mathematical Models for BWR Stability Calculations

This section presents some of the mathematical models that are commonly used for stability calculations. The purpose of this section is to point out the approximations and limitations for these models rather than to provide a complete reference of equations and correlations, which would be outside of the scope of this report. This section uses a significant number of *buzz words*, whose definitions are also beyond the scope of this document. For convenience to the reader, the first introduction of these buzz words is in italics.

4.1 Numerical Approximations for the Solution of Partial Differential Equations

The main approximation of all models used for stability evaluation comes from the fact that the conservation laws that must be satisfied by the variables of interest are typically expressed as partial differential equations (PDEs). Numerical mathematics, however, is well suited to solve ordinary differential equations (ODEs); thus, approximations are required to solve the physical problems numerically.

4.1.1 Nodal Approximations

The most commonly used approximation to reduce a PDE to a set of ODEs is to discretize the space variables by creating a group of *nodes*. The following steps are involved in this process:

1. Define a *mesh* of nodes that cover all the space of interest. This step is commonly referred to as a *nodalization* process.

2. Define *node-averaged values* for all the variables that have a space dependence.

3. Define *boundary conditions* that are consistent for the mesh chosen.

4. Approximate the space derivatives in the original PDE by relations between the node-averaged values. For example, the first-order space derivative may be approximated by the difference between the node-averaged values of two adjacent nodes divided by their distance. The result of this step is a set of algebraic equations that relate all the node-averaged values to each other and to their time derivatives.

5. Solve for the set of ODEs defined in step 4.

The accuracy of a nodal approximation depends on how coarse the nodalization is: the finer the mesh, the better the result (if one does not consider truncation errors due to the finite number of digits used by computers to represent real numbers). Accuracy can also be improved by defining *optimized* node-averaged values in step 2, instead of simple averages or node-center values. These optimized values are chosen so that the original PDE is conserved inside the node itself. This type of approximation is often called *finite element*, and it allows for coarser meshes with improved accuracy.

4.1.2 Modal Approximations

Another approximation that is commonly used (often without recognizing it) is a *modal* type of numerical solution. In this approximation, a *shape* is assumed for the space-dependent part of the solution, and the space derivatives are calculated analytically based on this shape; this process results in an ODE with time being the only independent variable. For this approximation, the solution is assumed to be *separable* and equal to the product of two functions: one that is only a function of time and another (the shape function) that is only a function of space.

An example of this modal approximation is the commonly used *point kinetics* formalism for the neutron field dynamics. Within point kinetics, the time- and space-dependent flux, $\Psi(t,r)$, is assumed to be equal to the product of a time-dependent flux level, $n(t)$, times a shape function, $\Phi(r)$; therefore,

$$\Psi(t,r) = n(t)\ \Phi(r) \qquad (4\text{-}1)$$

In this approximation, the space-dependence, $\Phi(r)$, is obtained from a *steady state* solution of the neutron field PDE (i.e., by forcing all time derivatives equal to zero). The steady state solution is then plugged into

the time- and space-dependent neutron field PDE to obtain an ODE for the time component, $n(t)$. In this way, the coefficients of the time-dependent ODE for $n(t)$ are a function of $\Phi(r)$.

A close inspection of Eq. (4-1) reveals that it is not a very good approximation in the sense that no deviation from the steady state space dependency, $\Phi(r)$, is allowed. Mathematicians, however, solved this problem long ago by realizing that the steady state solution of an *autonomous* space-dependent equation is typically *degenerate*, which means that there are an infinite number of spatial shapes, $\Phi_i(r)$ ($i = 1, \infty$), that satisfy the steady state equation. Thus, the general solution for the time- and space-dependent flux is not given by Eq. (4-1) but by

$$\Psi(t,r) = \sum_{i=1}^{\infty} n_i(t)\ \Phi_i(r) \qquad (4\text{-}2)$$

Each of the $\Phi_i(r)$ solutions is called a *spatial mode* or a *spatial harmonic*. The first harmonic or mode [the one called $\Phi(r)$ in Eq. (4-1)] is called the fundamental, and it is the one that dominates most transients. Spatial harmonics have some interesting mathematical properties, the most important of which is that they are *orthogonal* to each other

$$\int_v \phi_i(r)\phi_j(r)dr = 0\ ;\ if\ i \neq j \qquad (4\text{-}3)$$

A consequence of this orthogonality is that equations for each of the $n_i(t)$ can be derived that are independent of the other $n_j(t)$. In a stable *critical* reactor, all $n_i(t)$ have negative *eigenvalues* (i.e., they decay with time), so that only the contribution from the fundamental component is important and Eq. (4-1) becomes a good approximation. Under special circumstances (such as Xenon spatial oscillations, or out-of-phase instabilities in BWRs), the higher harmonics play an important role in the reactor dynamics.

The advantage of modal approximations over nodal approximations is that if one is interested in the temporal behavior of the fundamental or any other mode, this is precisely the quantity being computed and the results are exact. The disadvantage is that changes in spatial shape cannot be accommodated.

BWRs have a very complex dynamic behavior. To complicate the issue even further, the solution of the neutron dynamics blends itself quite easily to a modal approach (i.e., point kinetics), whereas a nodal approach is more appropriate for the thermohydraulics part of BWR dynamics. Thus, it is not unusual to see mixed nodal-modal calculations of BWR stability.

4.2 BWR Neutron Dynamics

Neutron dynamics define the behavior of the neutron field in a BWR, and, thus, they control the power generation term that feeds the thermohydraulics. One of the most exact representations of neutron dynamics is the time-dependent Boltzman Equation (also known as the neutron transport equation), which not only depends on time and space but also on energy and direction, for a total of eight independent variables. For obvious reasons, this equation cannot be solved directly numerically, and a significant number of approximations are required that are beyond the scope of this report.

The way in which the thermohydraulic calculations are coupled to the neutronics is of particular relevance to BWR stability calculations. This is accomplished by a reactivity calculation in the point kinetics formalism or by modifying the cross sections used in the diffusion or transport multidimensional calculations.

4.2.1 Reactivity Feedback in the Point Kinetics Formalism

Point kinetics, as stated before, is a modal approximation to the neutron dynamics. Indeed, the conventional point kinetics formalism solves for the time-dependent behavior of the fundamental mode of the neutronics. A rigorous derivation of the point kinetics formalism can be accomplished starting from the neutron transport equation and introducing the concept of adjoint flux, $\Phi^+(r)$. This derivation results in a series of formulas for all the space-independent

constants and variables that appear in the point kinetics equations for $n(t)$. The most important of these variables is the net reactivity feedback, $\rho(t)$, which is defined by Eq. (4-4),

$$\rho(t) = \frac{1}{V} \int_V \Phi^+(r)\ \rho(r,t)\ \Phi(r)\ dV \qquad (4\text{-}4)$$

where V is the core volume and $\rho(r,t)$ is the local reactivity feedback at position r, which is typically estimated as a function of changes in void fraction, α, and fuel temperature, T_f. Using the *linearized reactivity coefficients* $\partial\rho/\partial\alpha$ and $\partial\rho/\partial T_f$,

$$\Delta\rho(r,t) = \frac{\partial\rho}{\partial\alpha}(r,t)\ \Delta\alpha(r,t) + \frac{\partial\rho}{\partial T_f}(r,t)\ \Delta T_f(r,t) \qquad (4\text{-}5)$$

In the above equations, the local flux, $\Phi(r)$, is assumed to be normalized so that the integral over the whole volume, V, of the product of the flux times its adjoint is equal to one.

Radial Nodalization

Equations (4-4) and (4-5) would represent the optimal coupling from thermohydraulics to neutronics if the thermohydraulic solution were perfect and known at every position, r, in the reactor. Unfortunately, thermohydraulics is the most expensive part of the calculation because the solutions to many (sometimes ill-behaved) differential equations are involved. Thus, the thermohydraulics are often solved in fairly coarse meshes by grouping thermohydraulic channels in the radial direction. The process for coupling the point kinetics neutronics to the thermohydraulic calculations is shown schematically in Fig. 4.1 and is described mathematically in the following paragraphs.

To account for the coarse radial mesh, we must rewrite Eq. (4-4) as

$$\rho(t) = \frac{1}{V} \int_V \Phi^+(r)\ \rho(r,t)\ \Phi(r)\ dV = \frac{1}{A} \int_A \frac{1}{H} \int_0^H \Phi^+(r,z)\ \rho(r,z,t)\ \Phi(r,z)\ dz\ dA \qquad (4\text{-}6)$$

where A is the horizontal (i.e., radial) area of the core. The radial integration in Eq. (4-6) is then approximated by a sum over a group of channels (or thermohydraulic regions) that have similar power levels, Φ_i. In mathematical terms, this approximation becomes

$$\rho(t) \approx \frac{1}{N_b} \sum_{i=1}^{N_{Th}} N_i\ \Phi_i^+\ \rho_i(t)\ \Phi_i \qquad (4\text{-}7)$$

where N_b is the total number of bundles in the core, N_{Th} is the number of thermohydraulic regions (or channels) used for the calculation, N_i is the number of

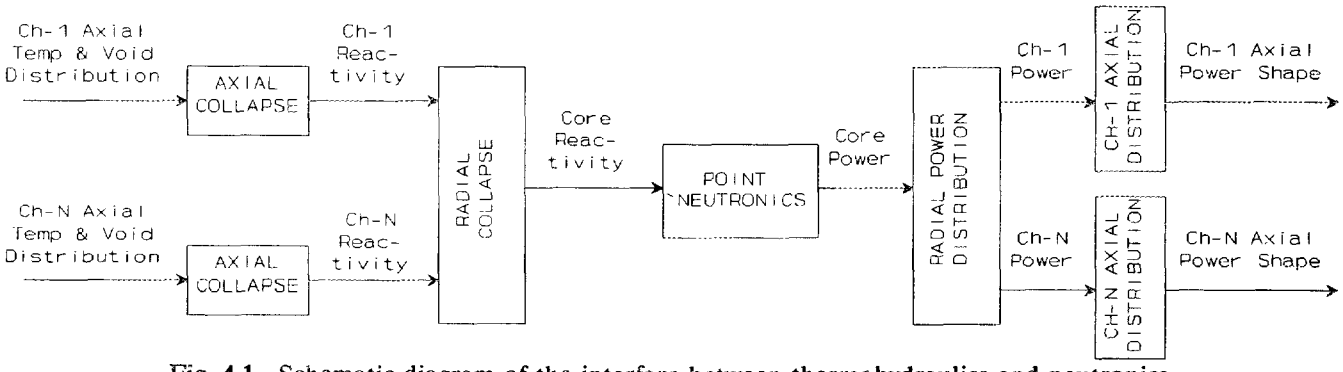

Fig. 4.1. Schematic diagram of the interface between thermohydraulics and neutronics for a typical BWR stability calculation using point kinetics

bundles in region i, and $\rho_i(t)$ is the reactivity feedback contribution from a single channel in region i, which is given by the following equation:

$$\rho_i(t) = \frac{1}{H} \int_0^H \varphi_i^+(z)\ \rho_i(z,t)\ \varphi_i(z)\ dz \qquad (4\text{-}8)$$

where $\varphi_i(z)$ is the axial flux distribution for thermohydraulic region i, which is normalized so that the integral over the height of the core of the axial flux times its adjoint equals one.

Axial Nodalization

Equation (4-8) again is solved by discretizing the axial dimension into a set of axial nodes. This axial nodalization is also fixed by the thermohydraulic calculation, and the number of nodes is typically determined by the accuracy desired. The reactivity feedback from a channel of thermohydraulic region i is then given by the following expression:

$$\rho_i(t) = \frac{1}{N_z} \sum_{j=1}^{N_z} \varphi_{ij}^+\ \rho_{ij}(t)\ \varphi_{ij} \qquad (4\text{-}9)$$

where $\rho_{ij}(t)$ is the local reactivity feedback contribution from axial node j in a single bundle of thermohydraulic region i, and it is calculated by an equation similar to Eq. (4-5).

Within one group diffusion theory, the adjoint flux is equal to the forward flux, and both are approximately proportional to the power generation term, P (if one assumes fairly constant fission material loading). Therefore, all the products of flux times its adjoint may be approximated by the power squared.

Thus, the general integral equation represented by Eq. (4-4) is approximated in most BWR stability point kinetics calculations by the following series of sums:

$$\rho(t) = \frac{1}{N_b} \sum_{i=1}^{N_m} N_i\ P_i^2 \left(\frac{1}{N_z} \sum_{j=1}^{N_z} P_{ij}^2\ \rho_{ij}(t) \right) \qquad (4\text{-}10)$$

where P_i is the normalized power of thermohydraulic region i and P_{ij} is the local power at axial node j of region i. This process is shown graphically in Fig. 4.1.

Note that in Eq. (4-10) the term $\rho_{ij}(t)$, which is inside both summations, is the product of the reactivity coefficients times the variations in void and fuel temperature [Eq. (4-5)]. A common mistake is to generate average reactivity coefficients and then multiply them by the time-dependent, spaced-averaged void fraction and fuel temperature. The result of this approximation is not equal to the result of Eq. (4-10) and can be in error significantly because of the strong nonlinear dependence of the reactivity coefficients. Whenever possible, an equation similar to Eq. (4-10) should be used.

4.2.2 Thermohydraulic Feedback in Multidimensional Diffusion Calculations

In multidimensional diffusion calculations, whether in one, two, or three dimensions, a process similar to the one described for the point kinetics case must be followed to estimate the thermohydraulic feedback. In principle, it is possible to generate a computer model with a one-to-one correspondence between the neutronic and thermohydraulic nodes. However, because the thermohydraulic part of the calculation is significantly more expensive than the neutronics, often the thermohydraulic mesh is defined based on representative regions that group many bundles with similar power density. Thus, an algorithm must be used to couple the thermohydraulic mesh to the neutronic mesh. In diffusion calculations, the concept of reactivity does not apply properly. Instead, the local cross sections of each neutronic node are varied as functions of the local void fraction and fuel temperatures based on static calculations that are performed at different void fractions, fuel exposure, and fuel temperatures.

One-dimensional (1-D) neutronic calculations (shown schematically in Fig. 4.2) typically conserve the

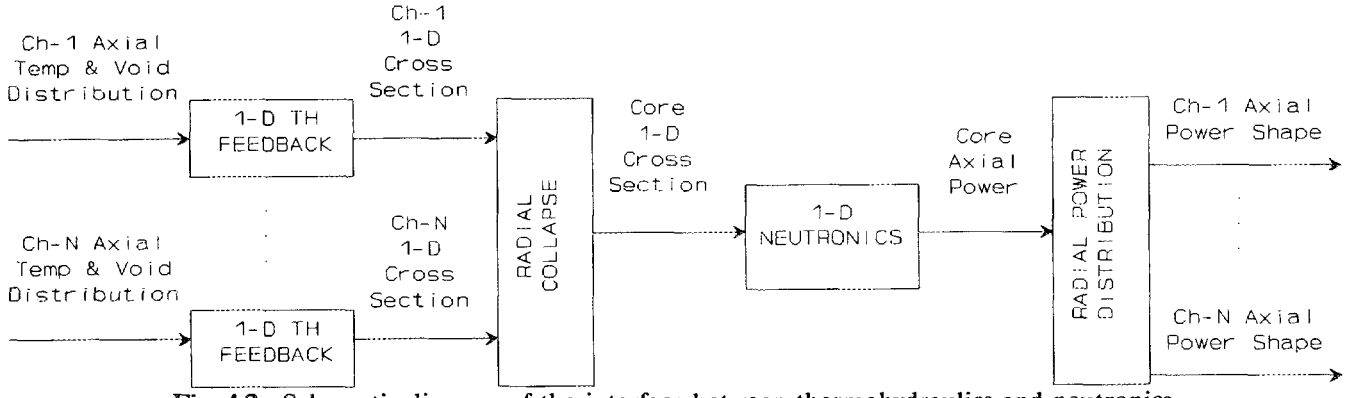

Fig. 4.2. Schematic diagram of the interface between thermohydraulics and neutronics for a typical BWR stability calculation using 1-D neutronics

axial direction in BWR stability calculations. In this way, the propagation of the density wave and its effect on the local power density can be modeled. To perform these calculations, the three-dimensional (3-D) thermohydraulic feedback must be collapsed into effective 1-D cross sections. Similarly, as in the case of the reactivity feedback, the optimal way to collapse cross sections is to use a flux adjoint weighing as shown mathematically in Eq. (4-11):

$$\Sigma(z,t) = \frac{1}{A} \int_A \Phi^*(r,z)\ \Sigma(r,z,t)\ \Phi(r,z)\ dA \qquad (4\text{-}11)$$

where the time-dependent local 3-D cross section, $\Sigma(r,z,t)$, is updated based on the local void fraction and fuel temperature calculated in the thermohydraulic mesh, and then collapsed to 1-D cross sections, $\Sigma(z,t)$, based on Eq. (4-11).

As in the case of point kinetics, the integral in Eq. (4-11) is replaced by a summation over the thermohydraulic channels, so that the 1-D cross section, $\Sigma(z,t)$, is estimated as

$$\Sigma(z,t) \approx \frac{1}{N_b} \sum_{i=1}^{N_{Th}} N_i\ P_i^2(z)\ \Sigma_i(z,t) \qquad (4\text{-}12)$$

where $\Sigma_i(z,t)$ is the cross section of thermohydraulic channel i. Similarly, as in the case of the reactivity feedback in point kinetics, a common mistake is to average first the radial void distribution and then estimate radially averaged cross sections. This mistake may underestimate the thermohydraulic feedback significantly because of the nonlinear nature of the process.

In 3-D neutronic calculations, the neutronic mesh is typically (although not always) smaller than the thermohydraulic mesh; thus, many neutronic nodes receive the same thermohydraulic feedback (especially when a limited number of thermohydraulic regions are used). The process to estimate the thermohydraulic feedback in 3-D calculations is shown schematically in Fig. 4.3. The key approximation in 3-D calculations is that only a few thermohydraulic regions are typically modeled; therefore, 3-D calculations require one algorithm to convert the 1-D cross section feedback calculated for each region to the finer neutronic mesh and another algorithm to collapse the fine 3-D power to region-averaged axial power shapes.

The selection of the number of thermohydraulic regions and the association between the finer neutronic nodes to the coarser thermohydraulic nodes are a key process in 3-D neutronics. This is especially true when inherent symmetries are used to reduce the problem dimensionality. It is not uncommon to perform 3-D quarter or even octant symmetry calculations where only an eighth of the core is really modeled. These symmetry approximations are appropriate for the fundamental mode of oscillation,

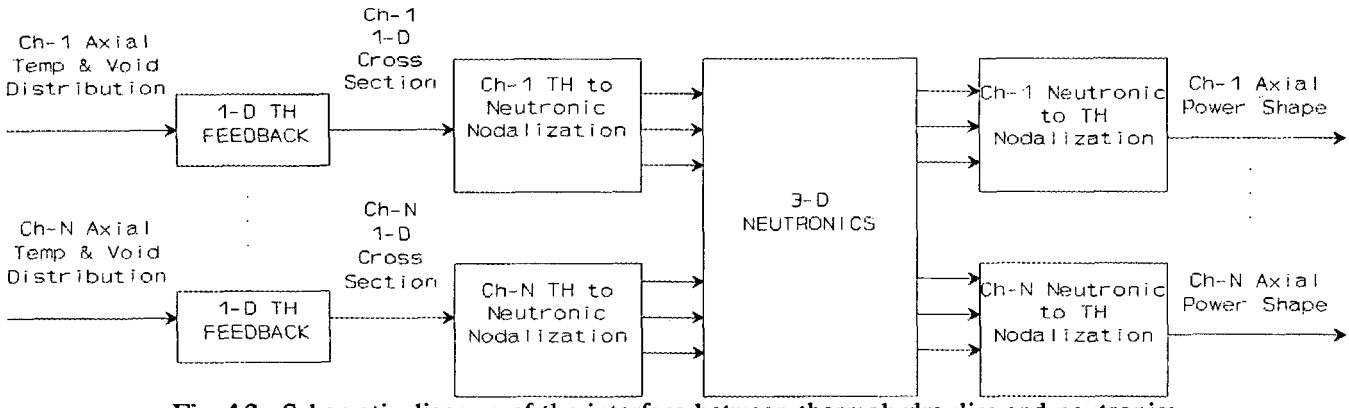

Fig. 4.3. Schematic diagram of the interface between thermohydraulics and neutronics for a typical BWR stability calculation using 3-D neutronics.

but they prevent numerically higher harmonics from developing; thus, 3-D octant calculations might show a stable reactor (in the calculated fundamental mode), while the out-of-phase mode is clearly unstable.

In spite of the problem described above, the 3-D solution should always be a more accurate approximation.

4.3 BWR Thermohydraulics

Thermohydraulics are by far the most complex part of BWR dynamics. Basically, one has to solve for the conservation of energy mass and momentum in the fuel and the coolant; however, because BWR conditions result in two-phase flow through a number of parallel fuel bundles, the solution to those conservation equations is quite complex.

As stated before, the thermohydraulics are not typically solved for each and every one of the bundles in the core, but a number of representative thermohydraulic regions are defined that group bundles with similar power and flow characteristics, and only one representative channel from each region is solved. The problem of coupling the calculations for different channels into a single core is shown schematically in Fig. 4.4. In this figure, we observe that the power and axial power distribution for each thermohydraulic region (or channel) is known from the neutronic calculation. Assuming an inlet flow, the thermohydraulic calculation estimates the temperature and void distribution that feeds back to the neutronic calculation through a reactivity feedback. The thermohydraulic part of the calculation also computes an outlet pressure. The outlet pressures from all regions are compared with each other, and the inlet flow to all regions is readjusted to achieve the same outlet pressure in all regions. The core outlet pressure also feeds back through the recirculation loop and alters the inlet flow. For instance, if the core pressure drop is too high, the core outlet pressure decreases, causing a reduction in inlet flow until the pressures are balanced.

4.4 Mode Orthogonality: Excitation of the First Axial Harmonic

An interesting fact that arises during BWR unstable oscillations is that the fundamental mode of oscillation does not appear alone, but it appears to be always accompanied by at least the first axial oscillation mode. From observations in actual reactor instability tests and 3-D code simulations, it appears that the fundamental mode always excites at least the first axial mode (and probably all higher axial mode harmonics). This fact is an apparent paradox because, in principle, the different harmonic modes are orthogonal to each other and, therefore, one cannot excite the other. This section attempts to explain this phenomenon. In a few words, this effect can be explained by the fact that the reactivity feedback is

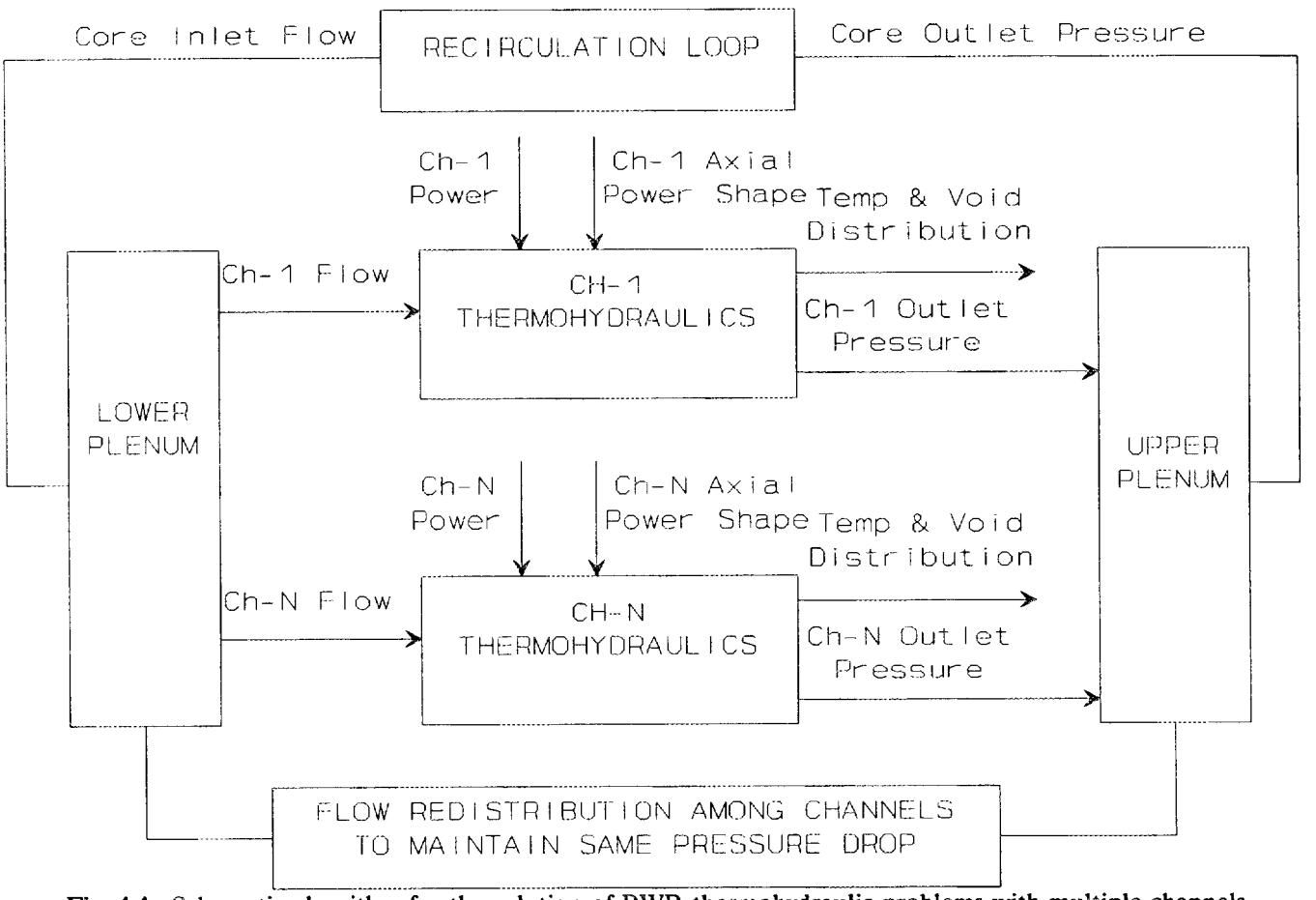

Fig. 4.4. Schematic algorithm for the solution of BWR thermohydraulic problems with multiple channels

nonlinear and, thus, linear mode orthogonality theorems do not apply.

To simplify the problem, we will assume a homogeneous, 1-D problem, where diffusion theory is applicable. In that case, the time- and space-dependent neutron flux, $\Psi(t,z)$, is given by the equation

$$\frac{1}{v}\frac{\partial \Psi(t,z)}{\partial t} = D\frac{\partial^2 \Psi(t,z)}{\partial z^2} + \Pi(t,z)\ \Psi(t,z) \qquad (4\text{-}13)$$

where D is the diffusion coefficient. The production operator, $\Pi(t,z)$, is a function of the fission and absorption cross sections, and it contains implicitly all the feedback terms (i.e., the cross sections depend on the local void fraction and fuel temperature). To simplify, we will assume that the feedback is directly proportional to the local neutron flux, $\Psi(t,z)$, as

$$\Pi(t,z) \approx \Pi_0 + \Pi_1\ [\Psi(t,z) - \Phi_0(z)] \qquad (4\text{-}14)$$

where $\Phi_0(z)$ is the steady state neutron flux and Π_0 and Π_1 are the linear and nonlinear components, respectively, of the production operator.

Following standard linear theory, we would assume that the neutron flux, $\Psi(t,z)$, is separable into two components: a time-dependent term, $n(t)$, and a space-dependent term, $\Phi(z)$. Again, following standard linear theory, we solve for the steady state eigenvalue

problem of Eq. (4-15), which results in a set of eigenvalues, λ_i, and eigenfunctions, φ_i, which are also called harmonic modes:

$$\lambda_i \; \varphi_i(z) = D \frac{\partial^2 \varphi_i(z)}{\partial z^2} + \Pi_0 \; \varphi_i(z) \qquad (4\text{-}15)$$

These harmonic modes are orthogonal to each other, and they form a complete set because Eq. (4-15) is of the *Sturm-Liouville* type. Therefore, the relation of Eq. (4-16) is satisfied:

$$\begin{aligned} \int_0^H \varphi_i(z)\,\varphi_j(z)\; dz &= \delta_{ij} \\ \delta_{ij} &= 1 \;\; if \; i=j \\ \delta_{ij} &= 0 \;\; if \; i \neq j \end{aligned} \qquad (4\text{-}16)$$

Within linear theory, the general solution for the time- and space-dependent neutron flux would be given by Eq. (4-17)

$$\Psi(t,z) = \sum_{i=0}^{\infty} n_i(t) \; \varphi_i(z) \qquad (4\text{-}17)$$

where the time-dependent terms, $n_i(t)$, should be independent of each other; but, because of the nonlinear nature of the feedback, this is not the case. Let's assume, to further simplify the algebra, that only two harmonic modes are present:

$$\Psi(t,z) \approx n_0(t)\,\varphi_0(z) + n_1(t)\,\varphi_1(z) \qquad (4\text{-}18)$$

Substitution into the original Eq. (4-13), taking into account the steady state eigenvalue [Eq. (4-15)] to eliminate the space derivatives, and performing some straightforward algebra results in

$$\begin{aligned} \frac{1}{v}\left(\varphi_0 \frac{dn_0}{dt} + \varphi_1 \frac{dn_1}{dt}\right) &= n_0 \lambda_0 \varphi_0 \\ &+ n_1 \lambda_1 \varphi_1 + \Pi_1 \; [\; (n_0 - 1) n_0 \varphi_0^2 \\ &+ n_1^2 \varphi_1^2 + n_1 (2n_0 - 1)\, \varphi_0 \varphi_1 \;] \end{aligned} \qquad (4\text{-}19)$$

where the term that multiplies Π_1 is caused by the nonlinear nature of the feedback.

Multiplying Eq. (4-19) by each of the eigenfunctions (i.e., harmonic modes), integrating over the core height, and taking into account the orthogonality relations, Eq. (4-16), one obtains a set of ordinary differential equations for the time-dependent part of the solution:

$$\begin{aligned} \frac{1}{v}\frac{dn_0}{dt} &= \lambda_0 n_0 + \Pi_1 [(n_0 - 1) n_0 \int_0^H \varphi_0^3 dz \\ &+ n_1^2 \int_0^H \varphi_0 \varphi_1^2 dz + n_1 (2n_0 - 1) \int_0^H \varphi_0^2 \varphi_1 dz \;] \\ \frac{1}{v}\frac{dn_1}{dt} &= \lambda_1 n_1 + \Pi_1 [(n_0 - 1) n_0 \int_0^H \varphi_0^2 \varphi_1 dz \\ &+ n_1^2 \int_0^H \varphi_1^3 dz + n_1 (2n_0 - 1) \int_0^H \varphi_0 \varphi_1^2 dz \;] \end{aligned} \qquad (4\text{-}20)$$

Note that if the feedback term did not exist (i.e., $\Pi_1 = 0$), the equations for $n_0(t)$ and $n_1(t)$ would be independent of each other. However, because of the nonlinear and space-dependent nature of the feedback, there are cross terms and $n_0(t)$ depends on $n_1(t)$ and viceversa. Note that the underlying cause of these cross terms is the fact that the cube integrals in Eq. (4-20) between orthogonal harmonics do not necessarily cancel. These cube integrals arise from the fact that the feedback term in Eq. (4-14) is space dependent; if the feedback were not space dependent, the space integrals containing cross terms would cancel and the modes would be truly orthogonal. Therefore, we can conclude that the harmonic modes are not, in general, orthogonal to each other during the oscillations, even though their space dependence (i.e., the steady state solutions) are orthogonal and they form a complete set.

Therefore, although the excitation of the axial harmonics during fundamental mode instabilities came as a surprise when first observed in tests and 3-D and 1-D calculations, this effect is not unusual and should have been expected because it derives directly from the theory. This section shows mathematically that the excitation of these axial harmonics is caused by the nonlinear and space-dependent nature of the reactivity (or cross section) feedback.

Equation (4-20) warrants further study. If we are interested only in the onset of linear instability, we can study the behavior of Eq. (4-20) under small perturbations around its equilibrium conditions ($n_0 = 1$, $n_1 = 0$). Linearizing Eq. (4-20) results in Eq. (4-21)

$$\frac{1}{v}\frac{d\delta n_0}{dt} = \lambda_0 \delta n_0 + \Pi_1 [\ \delta n_0 \int_0^H \varphi_0^3 dz + \delta n_1 \int_0^H \varphi_0^2 \varphi_1 dz$$

$$\frac{1}{v}\frac{d\delta n_1}{dt} = \lambda_1 \delta n_1 + \Pi_1 [\ \delta n_0 \int_0^H \varphi_0^2 \varphi_1 dz + \delta n_1 \int_0^H \varphi_0 \varphi_1^2 dz \qquad (4\text{-}21)$$

Furthermore, we notice that some cubic-type integrals are zero if the odd harmonics are symmetric; thus, the integral of $(\varphi_0^2\ \varphi_1)$ is zero under most circumstances (e.g., $\int \cos^2(\pi z/H)\ \sin(2\pi z/H)$ is equal to zero). Thus, under those conditions, the linearized equation becomes Eq. (4-22)

$$\frac{1}{v}\frac{d\delta n_0}{dt} = \lambda_0 \delta n_0 + \Pi_1 \delta n_0 \int_0^H \varphi_0^3 dz$$

$$\frac{1}{v}\frac{d\delta n_1}{dt} = \lambda_1 \delta n_1 + \Pi_1 \delta n_1 \int_0^H \varphi_0 \varphi_1^2 dz \qquad (4\text{-}22)$$

Therefore, the linearized problem does not have cross terms (at least in first approximation), and it makes sense to study the linear stability of each individual mode as suggested previously in this report. However, when nonlinear time domain calculations are performed beyond the linear instability threshold, cross terms cannot be neglected, and the equivalent of the full Eq. (4-20) must be used so there will be cross excitation among harmonics.

5 BWR Linear Behavior: Transfer Functions

Boiling water reactors behave linearly most of the time; nonlinearities become relevant only when an instability occurs and large amplitude oscillations develop, leading to a limit cycle caused by the excitation of these nonlinearities. Thus, it makes sense to describe the BWR behavior using linear transfer functions. This section presents some typical transfer functions calculated using the linear frequency domain code LAPUR.[5]

To maintain some consistency, all the transfer functions presented in this section correspond to a single LAPUR calculation of the LaSalle instability event on March 1988. The following reactor conditions were used for this simulation: power, 1465 MW_{th}; flow, 29.82 Mlb/hr; pressure, 964 psi; and inlet enthalpy, 503.5 BTU/lb. Six thermohydraulic regions (or channels) were used for the calculation, and Table 5.1 summarizes some of their conditions. Thermohydraulic channel 1 has the highest power, and channel 6 has the lowest. Channels 1 through 5 represent the core center, and channel 6 represents the periphery channels with reduced power and increased inlet restriction to minimize their flow. It should be noted that the conditions for the LaSalle event resulted in a fairly skewed radial power distribution that can be observed in Table 5.1. This skewed radial power distribution, along with a fairly bottom-peaked axial power shape, was probably the main cause of the observed instability. With this conditions, the LAPUR code predicts unstable conditions with a decay ratio of 1.05.

Figure 5.1 shows the closed-loop transfer function that relates external reactivity perturbations (measured in $\%\Delta k/k$) to changes in reactor power (normalized to the steady state power, which in this case is 1465 MW_{th}). We observe that there is a fairly large amplitude peak in the gain plot at about 0.4 Hz; this indicates that the reactor conditions are close to the instability boundary. The fact that the phase plot has a positive 180° shift at about the same frequency (0.4 Hz) indicates that this reactor condition is unstable.

The general shape of this transfer function is typical in that the gain plot increases at low frequency because of the presence of a low-frequency closed-loop zero. Then it peaks at about 0.5 Hz, and finally it flattens out at higher frequencies. The main features of the closed-loop transfer function are summarized in Figs. 5.2 and 5.3. Figure 5.2 shows a typical closed-loop reactivity to power transfer function in a Bode-type representation, and Fig. 5.3 is a root locus that shows the location in the complex plane of the main poles and zeros of the closed-loop reactivity to power transfer function as a function of an artificial parameter, which is the overall gain of the feedback loop. The most relevant poles are the two

Table 5.1. Description of thermohydraulic regions used for the LaSalle simulation

	Thermohydraulic Region Number (for Analysis)					
	Ch-1	Ch-2	Ch-3	Ch-4	Ch-5	Ch-6
Relative Power	144%	124%	108%	89%	65%	37%
Number of bundles	179	48	228	116	104	92
Inlet Restriction	Low	Low	Low	Low	Low	High
Exit Quality	0.321	0.255	0.209	0.156	0.099	0.108

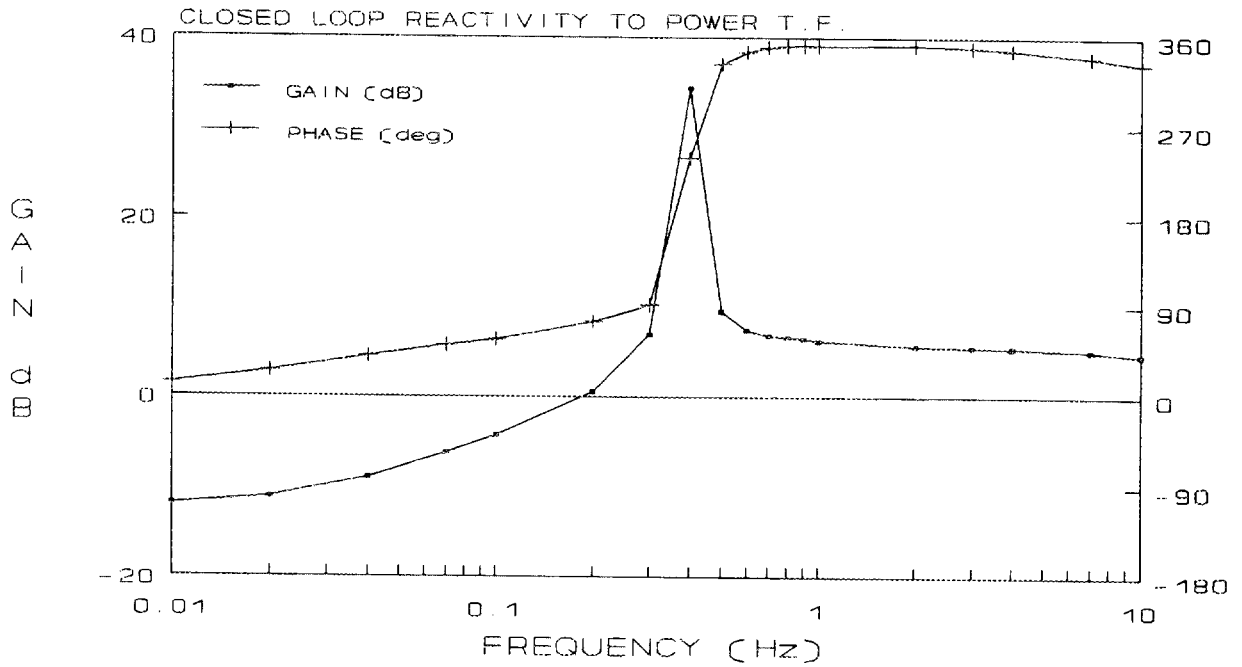

Fig. 5.1. Closed loop reactivity to power transfer function $(\%\Delta k/k)^{-1}$. Positive 180° phase shift at peak frequency indicates unstable conditions.

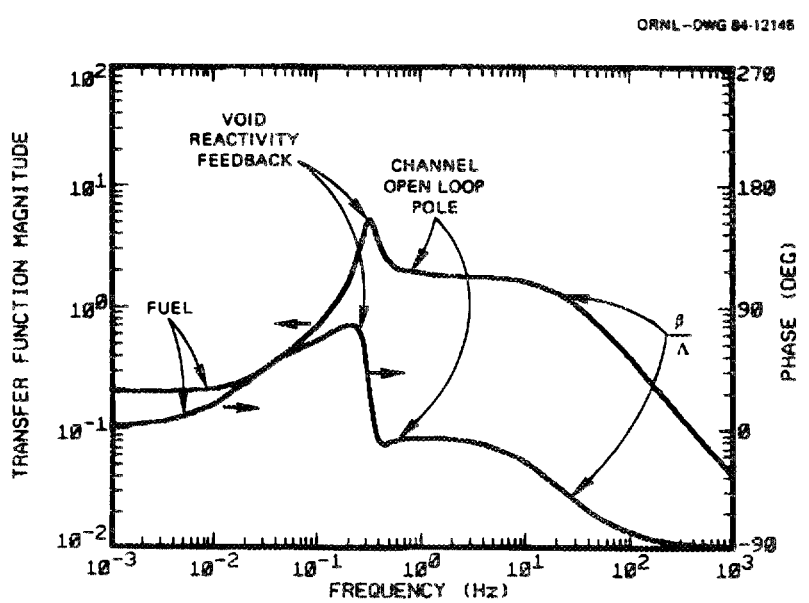

Fig. 5.2. Typical closed loop reactivity to power transfer function and observable features

complex poles at approximately 0.4 Hz; as seen in the root locus of Fig. 5.3, the poles start at the left-hand side of the plane (the stable side) and move along a line towards the right-hand side (the unstable half-plane). If the complex poles are in the right-hand plane, the reactor is unstable. Other relevant features are (1) the low-frequency closed-loop zero (at approximately 0.03 Hz) that is caused by the fuel time constant and its associated filtering effect and (2) the pair of complex closed-loop zeros (at about 0.4 Hz) that are caused by the channel thermohydraulics. These features can also be observed in Fig. 5.2.

Figure 5.4 shows the open-loop transfer function that represents the LaSalle event reactor conditions. The open-loop transfer function is the product of the forward (G) and the feedback (H) transfer functions. Since the G function has units of power divided by reactivity and the H function has units of reactivity divided by power, the open-loop transfer function (GH) is actually unitless. The point at which the gain plot crosses 1 (or 0 in dB units) or the phase plot

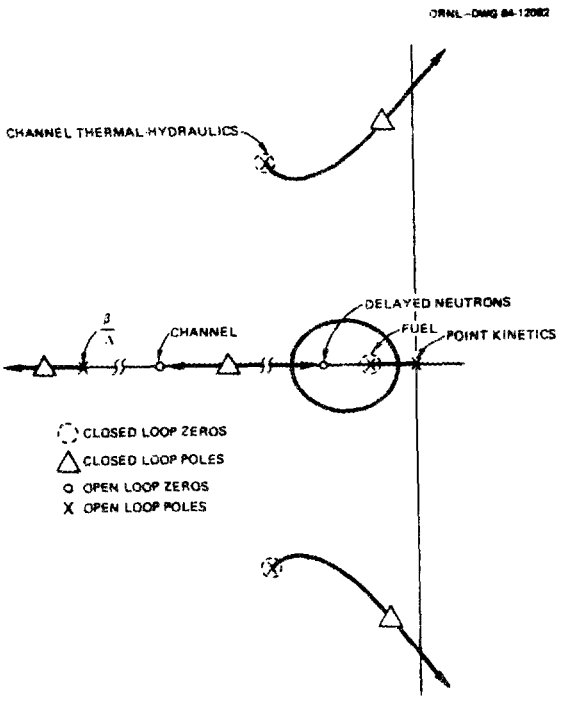

Fig. 5.3. Root locus of a typical BWR reactivity to power transfer function

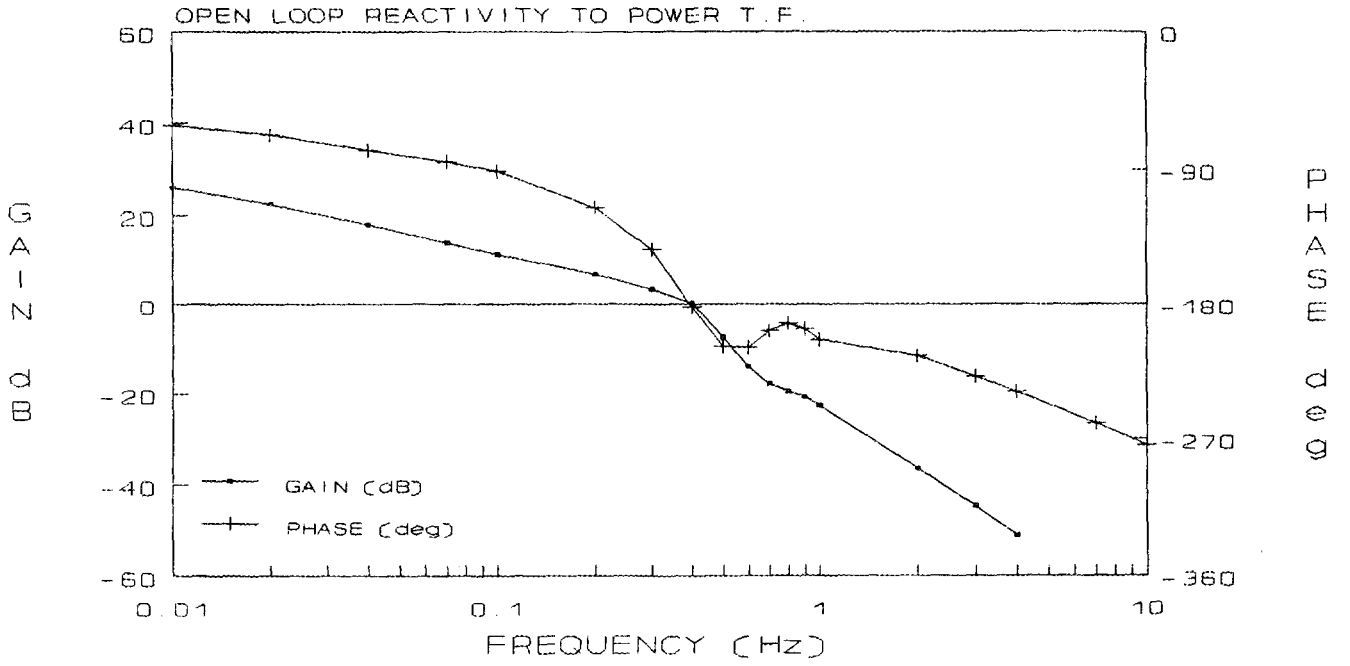

Fig. 5.4. Open-loop reactivity to power transfer function (unitless). Gain is greater than 0 dB when phase crosses -180°, indicating unstable conditions

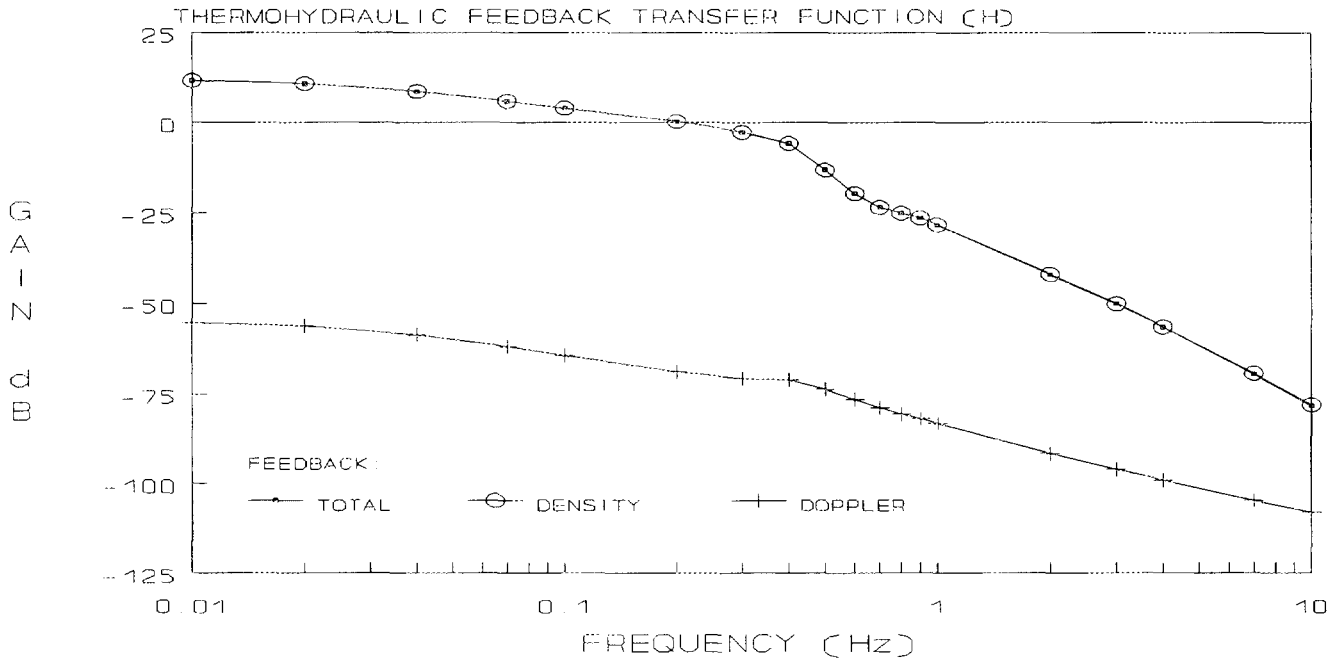

Fig. 5.5. Total feedback reactivity transfer function from power to reactivity (%Δk/k), showing the contribution from density and Doppler feedbacks

crosses -180° defines the system stability. In this case, we observe that the system is barely unstable (in fact it has a decay ratio of 1.05) because the gain is slightly higher than 0 dB when the phase is -180°.

Figure 5.5 shows a plot of the feedback transfer function gain, H, from power to reactivity for the LaSalle conditions. In this figure, the power is normalized to steady state and the reactivity has units of %Δk/k. Figure 5.5 also shows the relative contributions to H of the density reactivity and Doppler feedback mechanisms; the density feedback mechanism dominates the response and contributes more than 99% to the total value. Note that dBs are a logarithmic-type unit, where 20 dBs corresponds to a decade in linear scale. It is worthwhile to notice that the relative importance of the Doppler and density feedbacks changes as a function of frequency. As it can be observed in Fig. 5.5, the density feedback transfer function rolls off faster than the Doppler feedback contribution. The relative contribution from Doppler becomes more important for nonlinear large-amplitude oscillations.

The general shape of the feedback transfer function, H, can also be observed in Fig. 5.5, which shows a slow decrease at low frequencies but a fast roll-off close to the natural frequency of oscillation (0.4 Hz) of the reactor thermohydraulics. That roll-off at 0.4 Hz is also accompanied by a decrease in phase that contributes to the possibility of instabilities at this frequency.

Figures 5.6 and 5.7 show the contribution from each channel in a thermohydraulic region to the total density reactivity feedback. As it can be observed, the higher-power channels have a significantly higher contribution to the density reactivity feedback than the low-power channels. Note that dB units are logarithmic, so the differences in Fig. 5.6 are even larger than they appear. For example, Table 5.2 shows the relative gain of each of these transfer functions at 0.4 Hz, normalized to the gain of the high-power region (channel 1). In Table 5.2, we observe that region 3, which has a power level 108% higher than the average reactor, contributes only 18% to the total gain whereas region 1 contributes 41%.

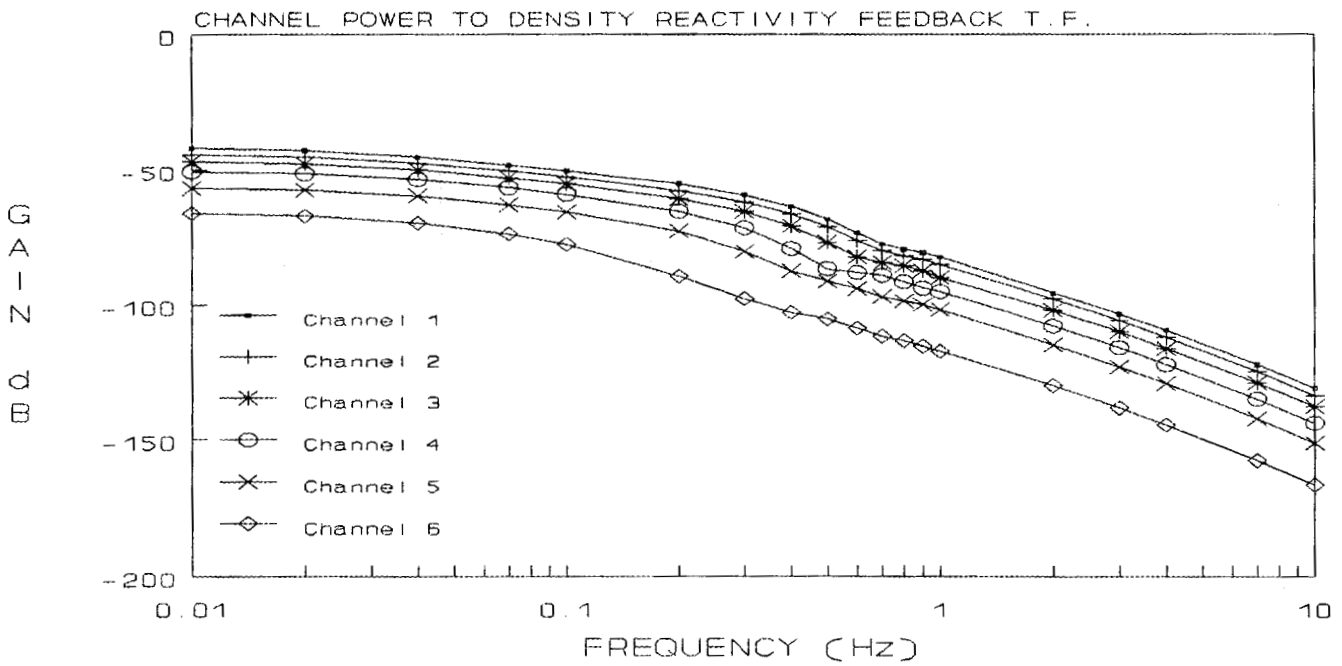

Fig. 5.6. Individual channel power to density reactivity transfer function gain (%Δk/k) for each thermohydraulic channel type. Channel 1 has the highest power and Channel 6 the lowest

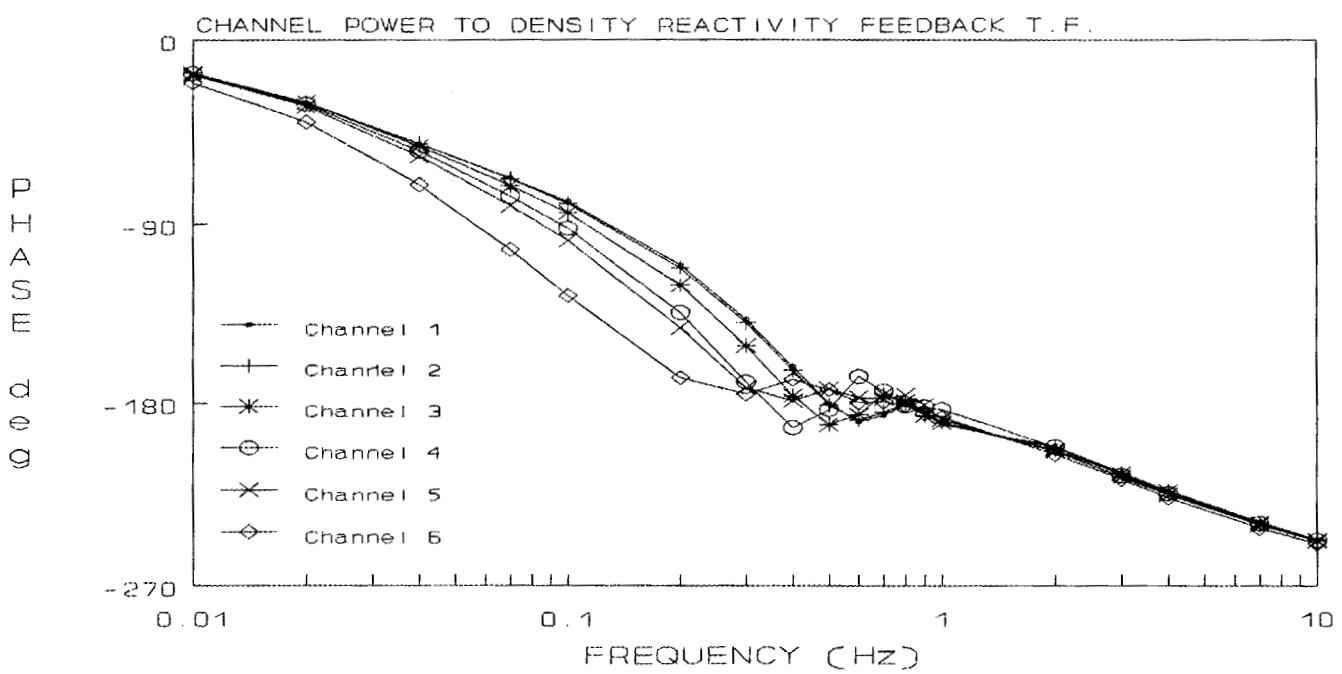

Fig. 5.7. Individual channel power to density reactivity transfer function phase (deg) for each thermohydraulic channel type. Channel 1 has the highest power and Channel 6 the lowest

Table 5.2. Gains of the individual channel power to density reactivity feedback transfer function at 0.4 Hz. Gains are normalized to the gain of the highest power channel.

	Ch-1	Ch-2	Ch-3	Ch-4	Ch-5	Ch-6
Relative Power	144%	124%	108%	89%	65%	37%
Number of bundles	179	48	228	116	104	92
Normalized gain	1.0	0.74	0.44	0.17	0.06	0.01
Overall Contribution	41%	31%	18%	7%	2%	0.4%

This implies that the relative contribution of a channel from region 3 is only 44% (18/41) of that from a channel in region 1.

The results presented in Table 5.2 and Figs 5.6 and 5.7 illustrate the need to model the radial power distribution fairly accurately. In particular, it is extremely important to represent properly the high-power channel distribution because these channels contribute most of the response. For example, the last row in Table 5.2 shows the relative contribution of each region to the overall density reactivity feedback if we assumed that all regions have the same number of channels. We observe that region 1 (the high-power region) would contribute 41% of the response, even if it had only 176 of 764 channels (23%). Thus, modeling the high-power channels is very important; however, we observe that all low-power channels could be lumped into a single region without much loss of accuracy because these channels do not contribute significantly to the overall feedback.

The underlying reason for the dominance of the high-power channels is that the density reactivity feedback is weighed by the local power square (i.e., the product of the neutron flux times its adjoint); furthermore, the density variations are proportional to the local channel power (for instance, the high-power channel has more voids). Therefore, there is an almost third-power dependence of the density feedback on the local channel power that strongly favors the high-power channels.

An effect similar to the one observed above can be seen in the transfer function from individual channel flow to density reactivity feedback (Figs. 5.8 and 5.9). These figures show in log scale (i.e., dB) the relative contribution that changes of inlet flow make to the overall density reactivity feedback. As in Fig. 5.6, the channels from the high-power region dominate the response.

Figures 5.10 and 5.11 show the response of individual channel flows to changes in reactor power. The picture here is not as clearcut as in Figs. 5.6 through 5.9, and one must look at the phase plot (Fig. 5.11) to understand it. What we observe is that the responses of channels 1, 2, and 3 (the high-power channels) are out-of-phase with respect to the responses of the low-power channels (4, 5, and 6). This indicates that, following a power increase, there is a flow redistribution between channels to maintain the same pressure drop across all of them.

A typical BWR core is composed of a large number of independent bundles that are connected hydraulically at both ends by the upper and lower plena. Because of these large plena, the pressure drop across all bundles must be maintained equal among all channels, although not necessarily constant in time, so that low-power channels must have the same pressure drop as high-power channels. Thus, to maintain this boundary condition, the inlet flow in the high-power channels must oscillate significantly more than in the low-power channels. This effect is caused by the fact

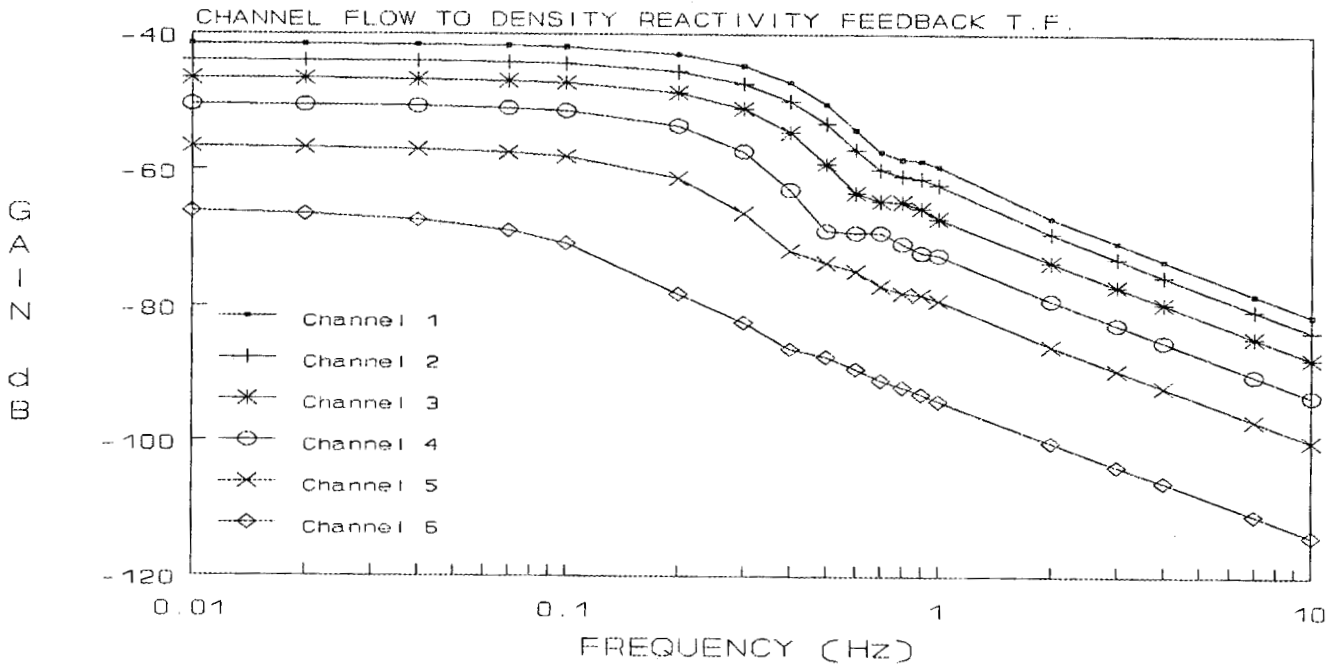

Fig. 5.8. Individual channel flow to density reactivity transfer function gain (%Δk/k) for each thermohydraulic channel type. Channel 1 has the highest power and Channel 6 the lowest

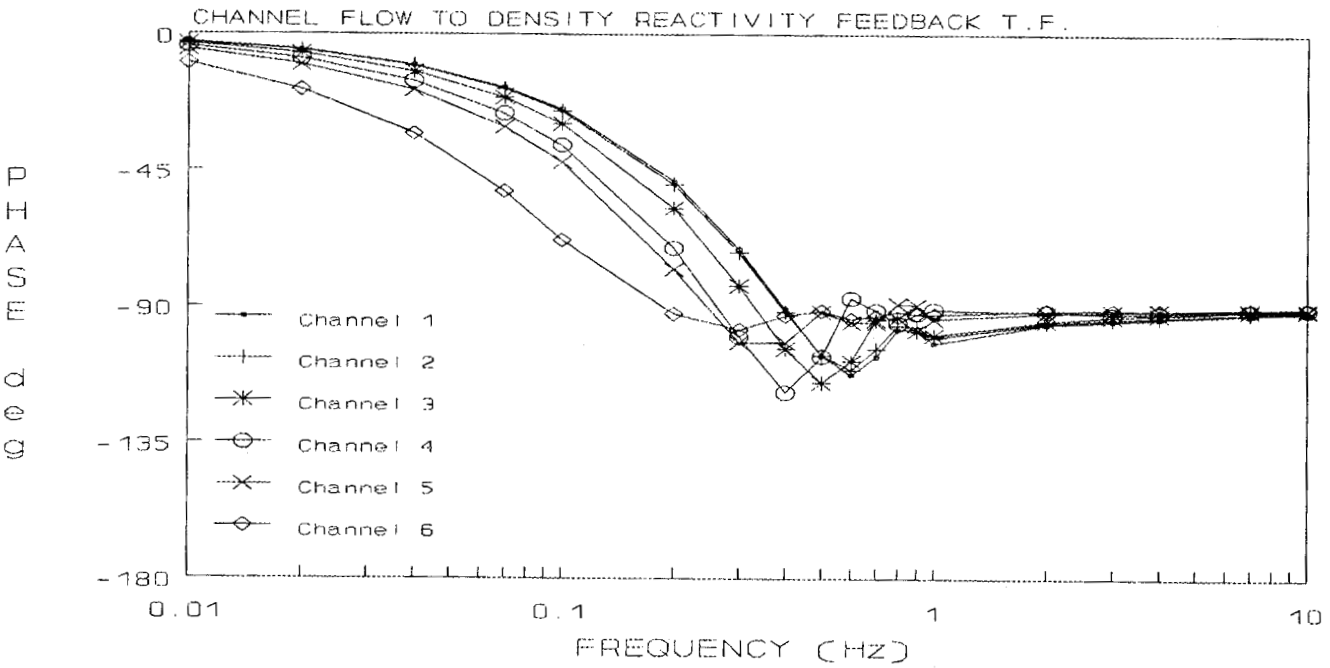

Fig. 5.9. Individual channel flow to density reactivity transfer function phase (deg) for each thermohydraulic channel type. Channel 1 has the highest power and Channel 6 the lowest

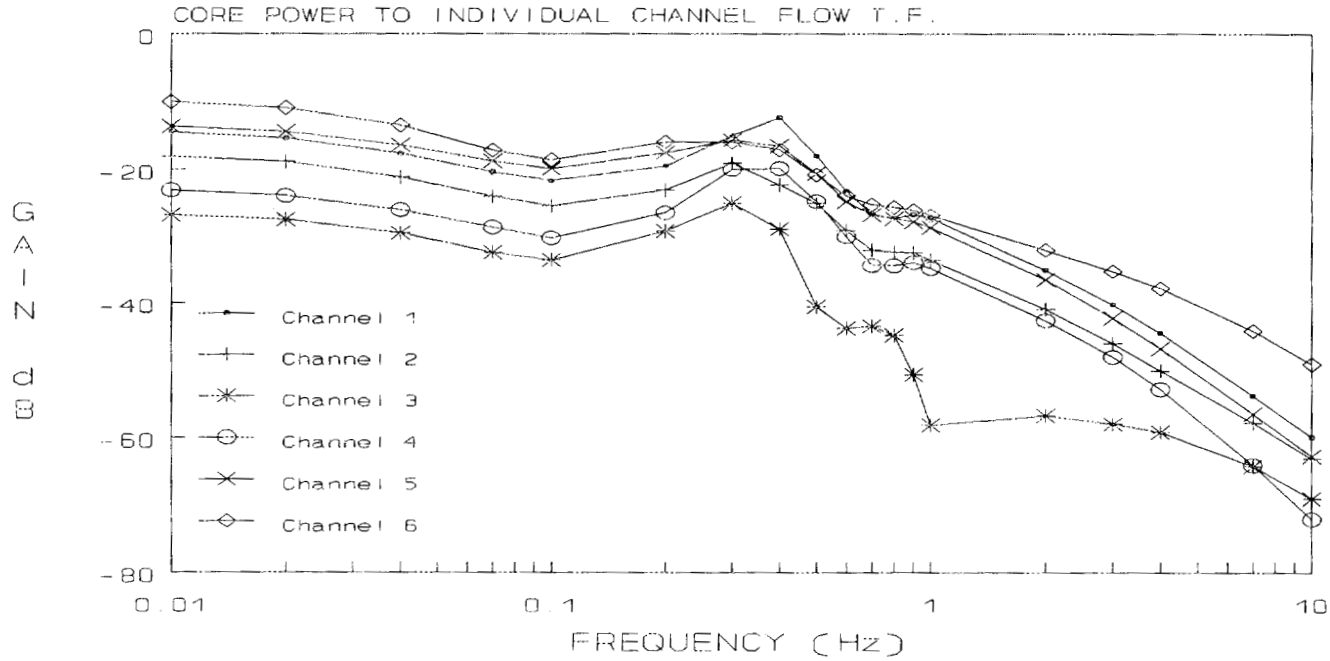

Fig. 5.10. Core power to individual channel flow transfer function gain (normalized) for each thermohydraulic channel type. Channel 1 has highest power, Channel 6 lowest.

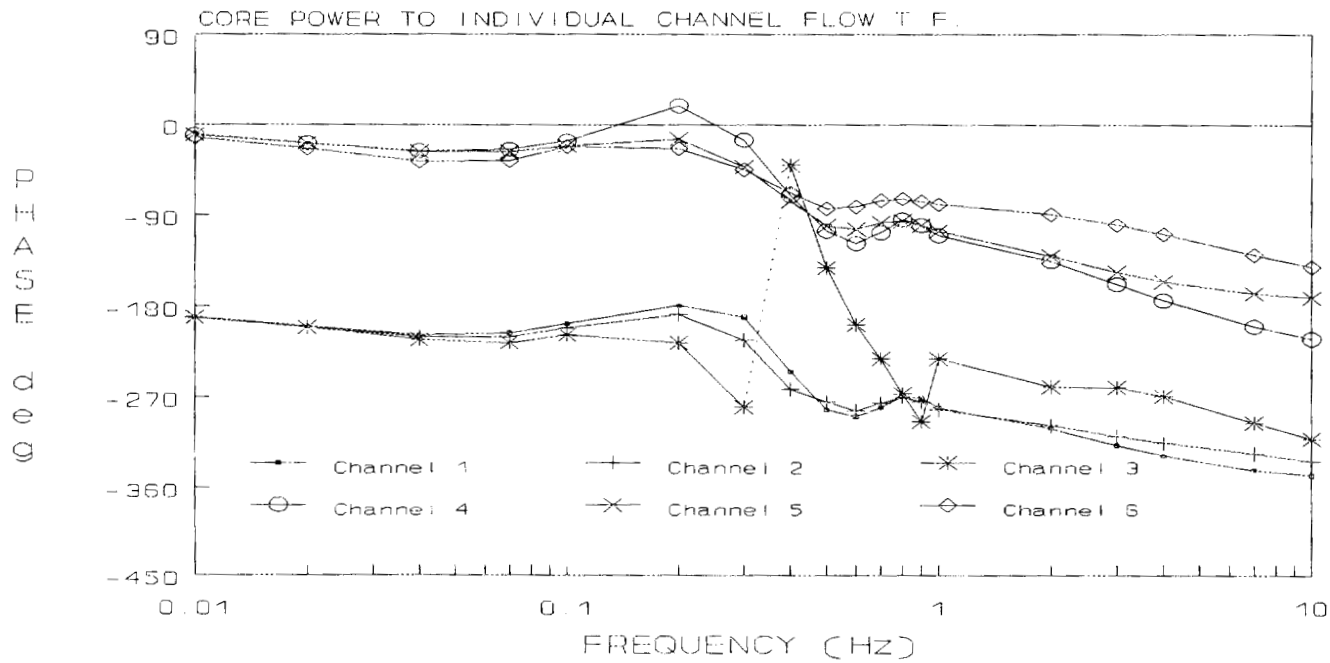

Fig. 5.11. Core power to individual channel flow transfer function phase (deg) for each thermohydraulic channel type. Channel 1 has highest power, Channel 6 lowest.

that the void oscillations are larger in the high-power channels. This has a very significant effect on channel pressure drop; thus, the inlet flow in the high-power channels has to compensate more for the increased flow oscillations, resulting in a more unstable configuration.

The effect of the radial power distribution can be observed in Table 5.3, which shows the decay ratio calculated by the LAPUR code for a core configuration formed by two thermohydraulic regions of an equal number of bundles. We observe that as the radial power distribution becomes more skewed (i.e., power is taken from region 1 to region 2), the reactor becomes more unstable. The conditions for Table 5.3 are 1500 MW_{th} power and 27 Mlb/h flow, with a sinusoidal axial power shape.

Table 5.3. Effect of checker board pattern loading on core-wide decay ratio

Relative Power		Decay Ratio
Region 1	Region 2	
100%	100%	0.54
80%	120%	0.81
60%	140%	0.98
40%	160%	1.35

An interesting result that highlights the effect of radial power distributions on inlet flow feedback can be observed in Table 5.4. From this table, we can conclude that a 1500 MW_{th} reactor with a skewed radial power shape is more unstable than a reactor condition with a higher power. For example, if the power is raised to 2100 MW_{th} (approximately 140% of 1500 MW_{th}) but only one thermohydraulic region is used, the calculated decay ratio is only 0.68, which is larger than the one-region decay ratio at 1500 MW_{th} (0.54) but smaller than the two-region (60%, 140%) reactor with only 1500 MW_{th} that results in a decay ratio of 0.98 (Table 5.3). This is a counterintuitive result. It says that if we take a reactor that operates at 2100 MW_{th} and reduce the power of half of the bundles (maintaining the rest of the bundles at constant power) so that the average power is 1500 MW_{th}, the resulting lower-power configuration is more unstable than the original high-power configuration.

The above effect can be explained by the effect the low-power channels have on the inlet flow feedback of the high-power channels. In the low-power channels, the void fraction does not oscillate as much as in the high-power channels following a reactivity perturbation. The large void fraction oscillation in the high-power channels would tend to produce large pressure drop oscillations; however, the

Table 5.4. Sensitivity of calculated core-wide decay ratio to recirculation loop gain for a uniform and a skewed radial power distribution

Relative Power		Decay Ratio if Recirculation Loop Gain is Multiplied by a Factor of					
Region 1	Region 2	0.	0.9	1.0	1.1	10.	100.
60%	140%	0.88	0.97	0.98	0.99	1.25	1.26
140%	140%	0.48	0.66	0.68	0.70	1.27	1.35

pressure drop across the high-power channels must equal that of the low-power channels. To accomplish this, the high-power channels inlet flow must have greater oscillation amplitude, resulting in an increased flow feedback that destabilizes these channels and the whole core.

The above theory is confirmed by the data in Table 5.4 that show the decay ratio as a function of the gain of the recirculation-loop pressure-drop-to-flow transfer. This gain may be increased physically by reducing the friction in the recirculation loop. If this loop has no friction, then it has an infinite gain and the pressure drop is maintained constant (and equal to the density plus pump heads) regardless of the amount of core inlet flow required. A large gain, then, essentially decouples the core channels from each other by forcing a constant-pressure-drop boundary condition. A small gain forces a constant core inlet flow, and the dynamic flow distribution between channels has a dominant effect. This effect is seen in Table 5.4. For high-gain values, the channels are uncoupled, and the one-region core with the highest power is more unstable. For low gain values, the two-region core (i.e., 60% and 140% powers) is more unstable than the one-region core because the low-power channels act as a source of flow to the high-power channels by oscillating their inlet flow out-of-phase.

In physical terms, we can explain this process as follows: when a perturbation of power causes an increase of voids in the high-power channels, the low-power channels increase their flow to attempt to have the same pressure drop as the high-power channels. This reduces the flow available for the high-power channels and, consequently, reinforces the original oscillation (i.e., more voids are produced). Thus this configuration is more unstable. For the case in which the recirculation loop has low friction (i.e., high gain), the increase in pressure drop in the high-power channels is compensated for by an increase in total flow, most of which is redirected through the low-power channels.

6 BWR Nonlinear Behavior: Limit Cycles

This section presents an interpretation of the physical mechanisms involved in the development of limit cycle oscillations in BWRs. Based on this interpretation, approximate correlations for some oscillation parameters are developed and shown to be largely independent of the particular reactor operating condition. The stability of the limit cycle is also studied. It is shown that the BWR limit cycle may become unstable and bifurcate. The bifurcation process leads to aperiodic (chaotic) behavior of the reactor power and causes the peak oscillation powers to be larger than those from a nonbifurcated limit cycle.

6.1 Background

Reactivity instabilities result in power oscillations that diverge from the steady state equilibrium point following a spiral trajectory in phase space. If BWRs behaved as linear systems, the oscillation trajectory would diverge indefinitely. The nonlinearities in the system, however, cause the oscillation to remain bounded as the trajectory converges to a limit cycle. The limit cycle is a particular periodic trajectory in phase space that attracts all other trajectories. If the oscillation trajectory is perturbed away from the limit cycle, it will eventually converge back to the limit cycle when the cause of the perturbation is removed. An example of a limit cycle in phase space can be seen in Fig. 6.1. In this figure, phase space is represented by the neutron flux and the excess fuel temperature. It can be observed that the trajectories diverge (i.e., spiral away) from the unstable equilibrium point but stay bounded and are attracted by the limit cycle trajectory. Mathematically, the limit cycle is caused by the nonlinearities in the system dynamics that have a stabilizing effect on the divergent oscillation. The main nonlinearity affecting BWR dynamic behavior was determined to be related to the power-dependence of the cross sections[7,8] (i.e, the void reactivity coefficient). In the point kinetics approximation, this nonlinearity is represented by the term ρ times n.

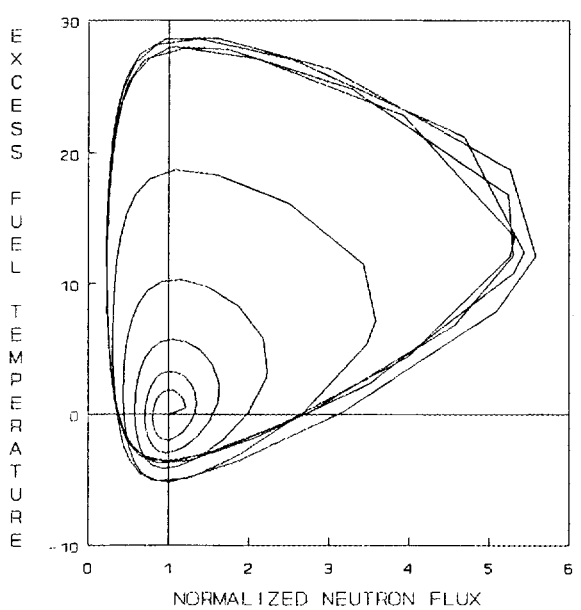

Fig. 6.1. Illustration of the development of a typical limit cycle in phase space

6.2 Reactivity Feedback During Limit Cycle Oscillations

Boiling water reactors are extremely complex nonlinear devices. To understand their behavior we must simplify their dynamics to a bare minimum. With this goal in mind, we should first attempt to understand their linear dynamic behavior. Figures 6.2 and 6.3 show the open-loop transfer functions of a typical BWR (computed using the LAPUR code[5]). A reactor is unstable if the open-loop gain is greater than 0 dB at the point where the phase is -180°. Figure 6.3 shows that the phase is only below -180° for a small range of frequencies around 0.4 Hz; therefore, unstable oscillations in BWRs must have a period of approximately 2.5 s, which is related to the bubble residence time in the core. We also observe in Fig. 6.2 that the magnitude of the reactivity feedback transfer function has a steep slope beyond 0.3 Hz. This implies that the reactivity feedback acts as a strong low-pass filter that damps high frequencies from the power oscillation. Thus, we can reach two conclusions from these simple observations:

1. If a limit cycle is developed by a BWR, the reactor power should follow a periodic oscillation

with a period of about 2.5 s (i.e., a frequency of approximately 0.4 Hz).

2. Regardless of the time shape of the power oscillation, the reactivity oscillation should be essentially sinusoidal. This is caused by the filtering effect of the reactivity feedback transfer function. No matter how many harmonics the power oscillation has, the reactivity feedback transfer function will filter out their contribution to the reactivity.

These two findings might seem somewhat irrelevant at first, but they allow us to simplify the limit cycle analysis dramatically. Typically, most of the modeling complications arise from the thermohydraulic feedback. If these two findings are applicable to any limit cycle case, then the feedback reactivity, $\rho(t)$, is given approximately by an expression of the form

$$\rho(t) = -\rho_0 + \rho_1 \sin(wt) \qquad (6\text{-}1)$$

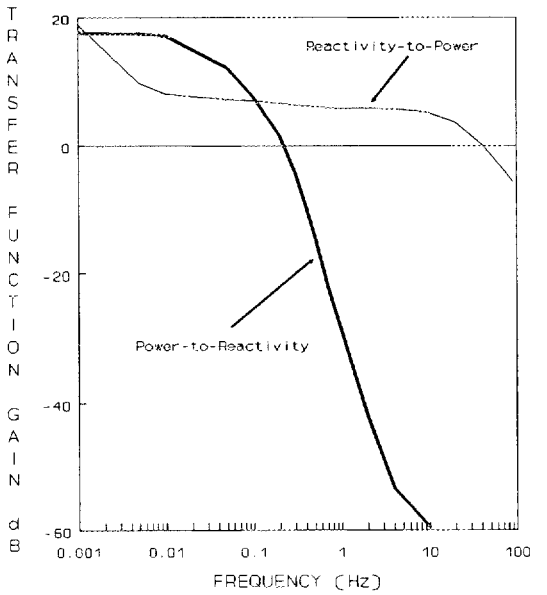

Fig. 6.2. Reactivity-to-power (G) and power-to-reactivity (H) transfer functions for a typical BWR

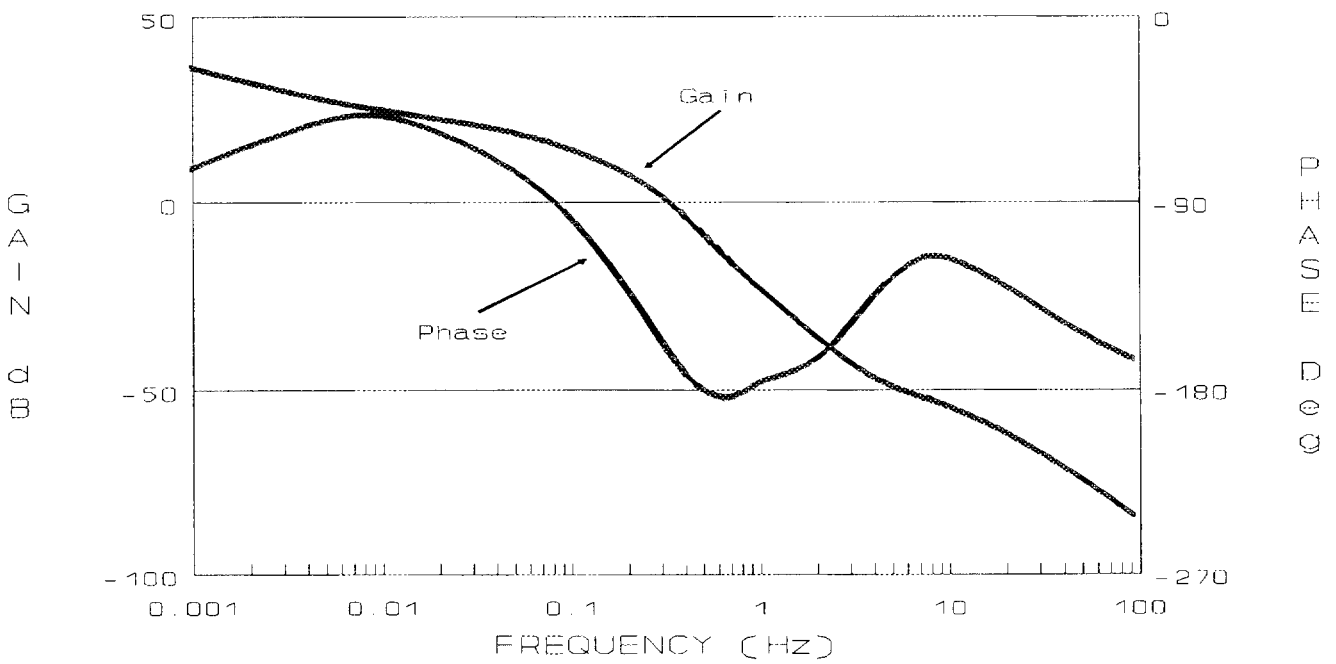

Fig. 6.3. Open-loop (GH) transfer function for a typical BWR

where ρ_o is the average reactivity value, ρ_1 is the amplitude of the oscillations, and w is the oscillation frequency that is approximately equal to 0.4 Hz.

The reduction of the complexity of a thermohydraulic model to a simple equation such as Eq. (6-1) allows us to perform very simple analyses that yield general correlations that are applicable with some degree of approximation to any BWR, as long as Eq. (6-1) holds. The parameters of these correlations now become ρ_o and ρ_1, instead of the physical geometry and cross sections of a particular reactor.

Equation (6-1) can be justified mathematically in the following manner: first, we know that a limit cycle oscillation is periodic. Thus, the power oscillation, $n(t)$, can be expanded in Fourier series without loss of generality as

$$n(t) = \sum_{k=0}^{\infty} A_k \cos(kwt) + \sum_{k=0}^{\infty} B_k \sin(kwt) \quad (6\text{-}2)$$

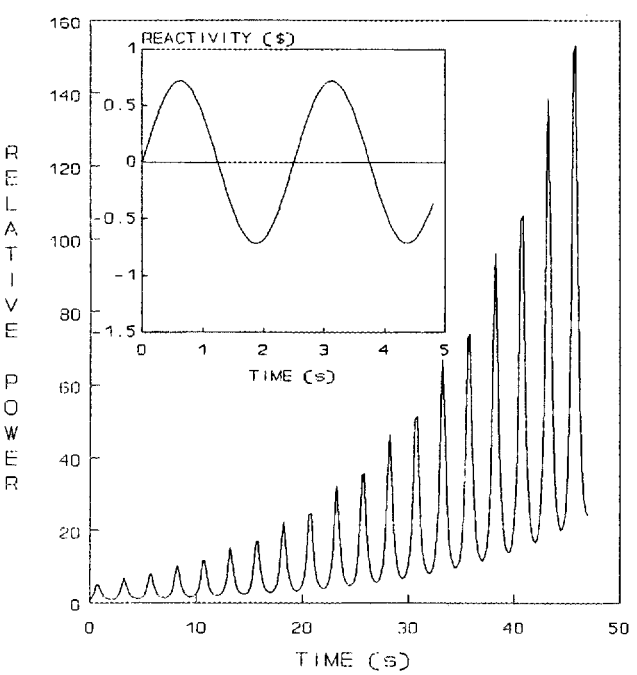

Fig. 6.4. Power response to sinusoidal reactivity with small bias

Because of the filtering effect of the fuel transfer function, large oscillations in power result in fairly small oscillations in heat flux from fuel to coolant, and the reactivity feedback transfer function can be considered to behave linearly.[8] Thus, the reactivity feedback can be approximated with good accuracy by the following expression:

$$\rho(t) = \sum_{k=0}^{\infty} H_k A_k \cos(kwt + \varphi_k) + \sum_{k=0}^{\infty} H_k B_k \sin(kwt + \varphi_k) \quad (6\text{-}3)$$

where H_k and φ_k are the gain and phase, respectively, of the feedback transfer function. Typical power feedback magnitudes (H_k) are 0.14 dollars per percent power change at 0 Hz, 0.007 \$/% at 0.4 Hz, and 0.0014 \$/% at 0.8 Hz.[5] Because the first two harmonics (k = 0 and k = 1) account for 99% of the feedback energy, higher harmonics can be neglected, and Eq. (6-3) reduces to Eq. (6-1) with the proper selection of initial phase lag. We shall use Eq. (6-1) to study the BWR limit cycle and to obtain some general correlations.

6.3 Reactor Response to Sinusoidal Reactivity Perturbations

The response of a nuclear reactor to sinusoidal reactivity perturbations has been well studied.[9,10] It is well known that a negative bias (i.e., $-\rho_o$) is required for the solution to exhibit bounded periodic solutions (i.e., limit cycles). For each value of ρ_1, there is only one value of ρ_0 that results in a limit cycle: if ρ_0 is too small, the oscillations diverge exponentially; if ρ_0 is too large, the oscillations converge to zero. The above effect can be seen in Figs. 6.4 and 6.5, which show the response of a point kinetics model (with typical BWR parameters) to a sinusoidal reactivity perturbation of the type in Eq. (6-1). In Fig. 6.4, the bias, ρ_o, is too small, and the resulting power oscillation diverges. In the case of Fig. 6.5, the bias is too large, and the power oscillation is damped and converges toward zero.

If the right amount of bias, ρ_o, is present for the particular amplitude of reactivity oscillation, ρ_1, we obtain the situation represented in Fig. 6.6, where the

power oscillation reaches and maintains a constant amplitude. The reactor behavior in this case is similar to that of a limit cycle caused by an instability. Thus, we conclude that in order to obtain periodic bounded power oscillations in a nuclear reactor, a relationship must be satisfied between the reactivity bias, ρ_o, and the reactivity oscillation amplitude, ρ_1. Physically, the reactivity bias is caused by an increase in average reactor power that increases with the oscillations until the reactor is subcritical enough to compensate for the divergent tendency imposed by the reactivity oscillation term, $\rho_1 \sin(wt)$.

To study the relationship between ρ_o and ρ_1, the model of ref. 8 was used to compute a large number of limit cycles with different oscillation amplitudes. In the model, which is described and validated in refs 7 and 8, the fuel dynamics are represented based on a single-node approximation, the channel thermohydraulics are modeled using a two-node representation, and the neutron dynamics are based on the point kinetic approximation. The model parameters used are those presented in ref. 8 with the exception of using six groups of delayed neutrons instead of one, and $K_o = -3.2769\text{x}10^{-3}$. Different limit cycle conditions were modeled by changing the feedback gain, K.

Table 6.1 shows a summary of the results of this analysis, presented as the values of ρ_o and ρ_1 required to obtain a limit cycle of amplitude N_{peak}. The linear decay ratio and inverse gain margins are also shown in Table 6.1. From these data, we can obtain the following correlation:

$$\rho_1^2 \approx 2\rho_0 + \rho_0^2 \qquad \textbf{(6-4)}$$

that relates reactivity bias required to maintain a bounded limit cycle with a particular reactivity oscillation amplitude. Equation (6-4) compares well with the analytic solution for small oscillations reported in ref 9 ($\rho_1^2 = 2\rho_0$; if $\rho_o << \$1$).

From the results shown in Table 6.1, we observe that the peak value of the neutron flux oscillations, N_{peak}, is related to ρ_1 through a correlation of the form

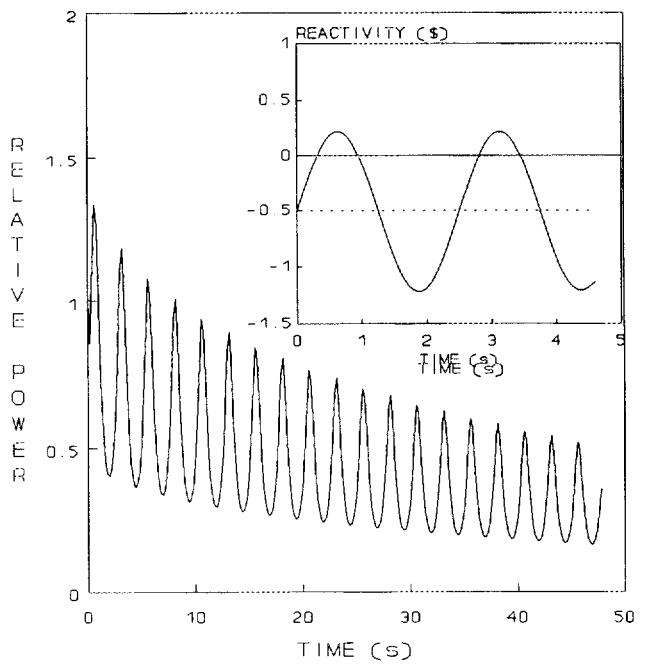

Fig. 6.5. Power response to sinusoidal reactivity with large bias

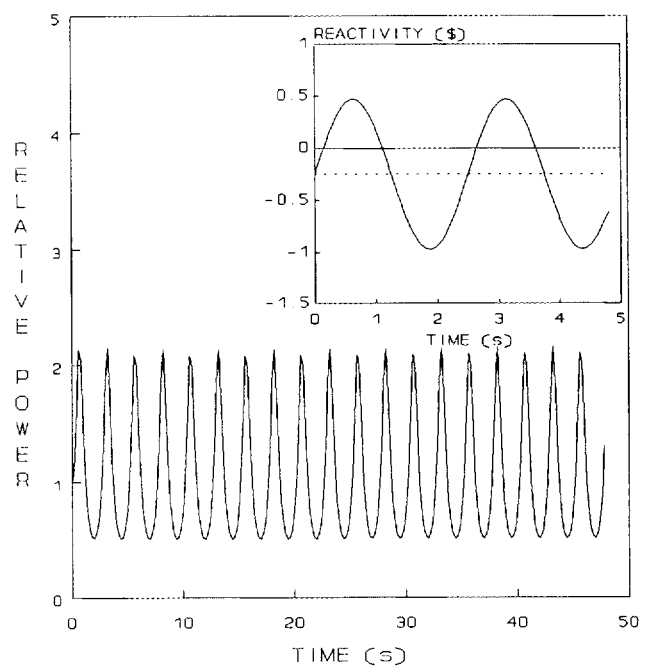

Fig. 6.6. Power response to sinusoidal reactivity with the right bias

$$\frac{(N_{peak} - N_0)}{N_0} \approx \rho_1 + 0.75\rho_1^2 - 0.14\rho_1^3 \qquad (6\text{-}5)$$

where N_o is the equilibrium flux. Note that Eq. (6-5) is valid only for reactivities satisfying Eqs (6-1) and (6-4), that is, for fully developed periodic limit cycles [Eq. (6-5) obviously cannot be applied to cases like those in Figs 6.4 or 6.5]. Equation (6-5) can be interpreted as the nonlinear reactor transfer function at the frequency studied (w = 0.4 Hz) and reverts to the linear gain (i.e., 1.0) for small values of ρ_1, as expected.

Numerical simulations appear to indicate that Eqs. (6-4) and (6-5) are independent of reactor parameters and, thus, general for any nuclear system where the point kinetics approximation is applicable.

6.4 Physical Mechanism of the BWR Limit Cycle

To have a self-sustained, periodic bounded oscillation of the power in a nuclear reactor, the reactivity feedback must oscillate sinusoidally and must have a negative bias of the appropriate magnitude. Indeed, this bias can be understood as the stabilizing mechanism for an unstable divergent oscillation. To understand this mechanism, we can follow, step-by-step, the development of a limit cycle in a BWR from the point of inception of the linear instability:

1. A moment before the instability event starts, the reactor can be assumed to be operating in a steady state condition with some particular power and flow. Because the reactor is critical at this point, the net reactivity is zero.

2. If by some change of conditions, the reactor suddenly becomes unstable in the linear sense, any small perturbation will result in diverging power oscillations that, in phase space, will spiral away from the equilibrium point similarly to the case presented in Fig. 6.1. Initially, the perturbation around the equilibrium point will be small enough so that the reactor will behave linearly and the oscillation will grow exponentially with a time constant equal to ***DR/w***, where ***DR*** is the decay ratio and ***w*** is the oscillation frequency.

Table 6.1. Calculated limit cycle parameters as a function of peak magnitude

K	DR	N_{peak}	ρ_0	ρ_1
1.0	1.00	100%	0.00	0.00
1.02	1.02	145%	0.063	0.36
1.05	1.08	182%	0.16	0.59
1.1	1.15	235%	0.32	0.87
1.2	1.30	330%	0.65	1.32
1.3	1.47	424%	0.98	1.72
1.4	1.62	515%	1.32	2.10
1.5	1.78	620%[a]	1.65	
1.6	1.93	980%[a]	1.90	
1.7	2.08	1350%[b]		
1.8	2.24	1800%[b]		
1.9	2.39	2400%[b]		
2.0	2.53	3200%[b]		

K = Inverse gain margin (see ref. 8)
DR = Decay ratio
N_{peak} = Peak oscillation value
ρ_0 = Reactivity bias in dollars
ρ_1 = Reactivity oscillation in dollars

[a] Solution has bifurcated (see ref. 8). Value reported is highest peak
[b] Solution is chaotic (see ref. 8). Value reported is highest peak

3. As the oscillation becomes larger, the nonlinearities in the system, and especially the ρ-times-n term, begin to grow in importance. These nonlinearities have the effect of "leaking" power between otherwise linearly orthogonal modes. In effect, the power that the instability is generating on the fundamental oscillation mode [*sin(wt)*] is distributed among other modes. In particular, some of the power of the fundamental mode "leaks" into the steady state mode (i.e, the average power). This increase in average power feeds back to the reactivity and generates a negative reactivity bias, ρ_o.

4. As the reactivity bias increases, the reactor becomes more and more subcritical and tends to damp out the unstable oscillation. When a sufficiently large degree of subcriticality is reached to cancel out the growth tendency imposed by the instability, a dynamic equilibrium is established and the limit cycle oscillation remains at a constant level.

Therefore, the underlying cause of the appearance of limit cycles that bound the oscillations of an unstable BWR is the increase in average power that accompanies the oscillations.

6.5 The Average Power Increase

We have seen that the average reactor power must increase during oscillations. Unfortunately, general correlations of the type of Eqs. (6-4) and (6-5) cannot be found for this increase because it depends on the particular reactor conditions. The procedure to estimate the average power increase for a given peak oscillation power is as follows:

1. Estimate, from Eq. (6-5), the value of ρ_1 required to establish the particular peak power, N_{peak}. Note that this procedure depends on the initial (or steady state) power, N_o. For example, almost twice as much reactivity, ρ_1, is required to obtain a peak power of 100 MW over the initial power, when operating at an initial power of 1000 Mw than at a power of 2000 MW. Thus, the value of ρ_1 depends not only on N_{peak}, but also on N_o.

2. Determine, from Eq. (6-4), the reactivity bias, ρ_o, required to maintain a periodic bounded oscillation with the particular value of ρ_1 obtained from step 1.

3. Determine the average power increase required to produce a reactivity bias of ρ_o. This is accomplished by dividing ρ_o by the steady state power reactivity coefficient, which depends on the particular reactor and operating conditions.

This procedure results in an approximate correlation for the average power increase, N_{ave}, of the form

$$N_{ave} = F_{ave}(N_{peak} - N_0) \qquad (6\text{-}6)$$

where F_{ave} is a proportionality factor that, for typical BWR parameters, is of the order of 0.015 to 0.02. Therefore, the average power increase is typically 1.5% to 2% of the value of the peak power minus the steady state power.

6.6 Limit Cycle Stability

Numerical simulations[8,11] have shown that as a parameter controlling the reactor's linear instability is increased, the limit cycle may become unstable and degenerate, through a cascade of period-doubling *pitchfork bifurcations*,[12] into a chaotic (i.e., aperiodic) sequence of power oscillations. In this regime, the power oscillations are aperiodic but remain bounded by a *strange attractor*.[12] It appears, however, that the oscillation amplitude (i.e., peak power) is increased by this phenomenon, and that the bifurcated limit cycle exhibits larger peak powers than extrapolation of the non-bifurcated limit cycle would predict. Thus, the understanding of the bifurcation phenomenon in BWRs is relevant to accident analysis where large peak powers may affect fuel integrity.

As seen in previous sections, if a positive disturbance is imposed on a limit cycle, the system nonlinearities create a positive average power increase that, through its reactivity effect, damps out the disturbance. An instability in this mechanism can occur if the average power increases too much during

a power peak and causes the next peak to decrease by an amount larger than the original disturbance. Thus, if a limit cycle should become unstable, an oscillation of double the original period will be established because the mechanism involves two full oscillation periods. In first approximation, the average power (<N>) and the reactivity bias, ρ_o, can be assumed proportional to the peak disturbance value, N_{peak}.

$$\frac{\Delta \rho_0}{\rho_o} \approx \frac{\Delta \langle N \rangle}{\langle N \rangle} \approx \frac{\Delta N_{peak}}{N_{peak}} \qquad (6\text{-}7)$$

Poincare maps were used in ref. 2 to study numerically the stability of the limit cycle and the bifurcation process. These maps are obtained by plotting the value of a power oscillation peak, N_2, versus the previous oscillation peak value, N_1. It has been shown in ref. 2 that this procedure results in a quadratic map similar to those studied by Feigenbaum.[12] An analytical expression for this map is the following:

$$N_2 = N_1 \; DR(N_1) \qquad (6\text{-}8)$$

where DR is the nonlinear decay ratio, which is a function of the oscillation amplitude. The equilibrium limit cycle is defined by $N_2 = N_1$, or $DR = 1.0$.

The stability of the limit cycle is guaranteed as long as the derivative of N_2 with respect to N_1 evaluated at the equilibrium point ($DR = 1.0$) is greater than -1.0 (i.e., the slope of the Poincare map is smaller than 45°). Taking derivatives in Eq. (6-8), we obtain

$$\frac{dN_2}{dN_1} = DR + N_1 \frac{dDR}{dN_1} \approx 1.0 + \frac{dDR}{dK} \frac{dK}{d\rho_0} \rho_0 \qquad (6\text{-}9)$$

where K is the inverse gain margin,[8] and we have made use of Eq. (6-7). Thus, the stability condition is

$$\rho_0 > \frac{-2}{\left(\frac{dDR}{dK} \frac{dK}{d\rho_0} \right)} \qquad (6\text{-}10)$$

From Table 6.1 we observe that the term dDR/dK evaluated around $DR = 1.0$ is approximately constant and equal to 1.43. The term $dK/d\rho_o$ is physically the change in gain of the neutron dynamics caused by a reactivity increase. For small perturbations around the limit cycle, this second term is approximately 1.0 dollars^{-1}. Thus, the condition for stability of the limit cycle can be approximated by

$$\rho_0 > \$-1.40 \qquad (6\text{-}11)$$

Using the correlations developed above, the stability condition can be expressed in terms of peak power. The result is that BWR limit cycles should be stable for peak power values of approximately less than 500% of equilibrium (i.e, initial) power. Beyond these limits, the bifurcation and chaotic regimes are established, and the result is larger peak powers than a nonbifurcated limit cycle study would predict.

7 Sensitivity to Physical Parameters

In this section we make a distinction between parameters that favor the development of instabilities of either of the two modes described (core-wide and out-of-phase) and parameters that favor one mode over the other. In general, though, the sensitivity of both modes to all parameters is similar, because the processes involved are alike.

7.1. Parameters Affecting the Core-Wide Instability Mode

In general, to decrease the stability in a BWR, there are two main approaches: (1) increase the neutronic feedback or (2) increase the instability of the density-wave mechanism. Most parameters affect the reactor stability in one way or another. Parameter effects are sometimes counterintuitive, so the best solution is to perform stability calculations at the actual operating conditions. Nevertheless, the following general ideas can be expressed about most parameters.

Average Void Fraction. This is the single most important parameter that affects BWR stability. Given two operating conditions, the one with the higher void fraction will have a stronger neutronic feedback (because of the increased density reactivity coefficient) and a larger two-phase pressure drop. Both effects tend to destabilize the reactor.

Axial Power Shape. The axial power shape has a strong influence on reactor stability. Bottom-peaked power shapes are more unstable because they tend to increase the axially averaged void fraction. In addition, void perturbations start at a lower axial level, which produces a larger delay. Under some conditions of extremely bottom-peaked power shapes, shifting power to the core bottom has been shown to have a stabilizing effect due to the effect of reducing the adjoint weighing in the upper, high-void-fraction content part of the core.

Radial Power Shape. Modeling the radial power shape is relevant to BWR stability calculations because of the inherent nonlinearities. Because of these nonlinearities, the most unstable channel (the one with higher power) tends to dominate the overall response, rather than being averaged with the low-power channel.

Void Velocity. Lower void velocities result in longer delay times for the density wave. Thus, given the same parameters, the operating condition with the lower flow should be more unstable.

Inlet Subcooling. Decreasing the inlet subcooling has two effects: (1) given a constant control rod position, it tends to increase the operating power level, which is a destabilizing effect; and (2) it raises the boiling boundary, thus decreasing the density-wave time delay. In most cases the destabilizing effect should dominate.

Fuel Gap Conductance. Increasing the gap conductance increases the amount of power deposited in the channel coolant during a neutron flux oscillation of a particular frequency. Thus, it has a destabilizing effect.

Fuel Isotopic Composition. The fuel isotopic composition has an indirect effect on BWR stability through its effect on the density reactivity coefficient. This effect depends on burnup and operating procedures, so it is difficult to predict.

7.2. Parameters that Favor the Out-of-Phase Instability Mode

To favor the out-of-phase instability mode over the core-wide mode, one should either reduce the subcritical reactivity value of the out-of-phase mode or increase the likelihood of out-of-phase density-wave oscillations. The following parameters accomplish these effects.

Low Geometric Buckling. The subcritical mode reactivity is directly proportional to the difference between the geometric bucklings of the fundamental and subcritical modes. Therefore, larger cores should be more susceptible to out-of-phase instabilities than smaller cores.

High Fission Cross Section. The subcritical mode reactivity is inversely proportional to the fission cross section. The higher the fission cross section is, the more likely the out-of-phase mode will be dominant.

As a rule of thumb, reactor conditions with many control rods in (i.e., at beginning of cycle) will have higher fission cross section and will favor the out-of-phase mode.

High Pressure Drop Across Channel. The out-of-phase density-wave mechanism is favored over the core-wide mechanism at higher pressure drops. This effect is caused by the increased flow feedback. Thus, high core pressure drops might result in out-of-phase oscillations.

High Flow Rate. A higher flow rate will favor the out-of-phase mode because of the increased friction pressure drop.

High Friction in Recirculation-loop Flow Path. Increasing the friction of the recirculation-loop flow path decreases the flow feedback for the core-wide mode and, therefore, favors the out-of-phase instability mode.

Highly-Bottom-Peaked Axial Power Shapes. For very highly-bottom-peaked axial power shapes, the density-wave flow instability mode is enhanced, while the reactivity or neutronic feedback is diminished because of a reduction of adjoint weighing at the upper part of the channel. As a rule of thumb, axial power shapes with peaking factors greater than 1.6 at the bottom are likely to result in out-of-phase instability modes.

Low Single-Phase Friction. Plants with loose inlet orifices will tend to favor density-wave flow oscillations and, thus, increase the likelihood of out-of-phase instability modes.

8. References

1. J. March-Leuba and B. Damiano, Susquehanna-2 Stability Measurements During Cycle 3, Oak Ridge Nat. Lab. Letter Report, ORNL/NRC/LTR-90/3, 1990.

2. R. T. Lahey and F. J. Moody, "The Thermal-Hydraulics of a Boiling Water Nuclear Reactor," American Nuclear Society Monograph, 1977.

3. E. Gialdi, et al., "Core Stability in Operating BWR: Operating Experience," Proceedings of SMORN-IV, Prog. Nucl. Energy, **15**, 1984.

4. NRC Bulletin 88-07 Supplement 1, Power Oscillations in Boiling Water Reactors, December 30, 1988.

5. P. J. Otaduy, "Modelling the Dynamic Behavior of Large Boiling Water Reactor Cores," Ph.D. Dissertation, University of Florida, 1979.

6. J. March-Leuba and P. J. Otaduy, "The Importance of Momentum Dynamics in BWR Neutronic Stability: Experimental Evidence," Trans. Am. Nucl. Soc., **50**, 563-564, 1985.

7. J. March-Leuba, "Dynamic Behavior of Boiling Water Reactors," Ph. D. Dissertation, The University of Tennessee, Knoxville, 1984.

8. J. March-Leuba, D. G. Cacuci, and R. B. Perez. "Nonlinear Dynamics and Stability of Boiling Water Reactors: Part I—Qualitative Analysis." Nucl. Sci. Eng. **93**, 111-123, 1986.

9. H. P. Smith, Jr. "Divergence of the Mean Power Level During an Oscillation Experiment." Nucl. Sci. Eng. **22**, 253-254, 1965.

10. Z. Akcasu, G.S. Lelouche, and L.M. Shotkin. Mathematical Methods in Nuclear Reactor Dynamics, Academic Press, 1971.

11. J. March-Leuba, D. G. Cacuci, and R. B. Perez, "Universality and Aperiodic Behavior in Nuclear Reactors," Nucl. Sci. Eng. **86**, 401-404, 1984.

12. M. J. Feigenbaum, "The Transition to Aperiodic Behavior in Turbulent Systems." Commun. Math. Phys. **77**, 1980.

Appendix A Nomenclature

Δ	increment operator
ρ or $\rho(t)$	reactivity
$\rho(r,t)$	reactivity contribution from location r [see Eq. (4-4)]
$\rho_i(t)$	reactivity contribution from thermohydraulic region i
$\rho_{ij}(t)$	reactivity contribution from axial node j in thermohydraulic region i
ρ_o	average reactivity value or bias [see Eq. (6-1)]
ρ_1	amplitude of sinusoidal reactivity oscillation [see Eq. (6-1)]
w	oscillation amplitude
α	void fraction
Φ or $\Phi(r)$	steady state neutron flux
Φ^+ or $\Phi^+(r)$	steady state neutron flux adjoint
Ψ or $\Psi(t,r)$	time-dependent neutron flux
Φ_i or $\Phi_i(r)$	i^{th} neutron flux harmonic
$d\rho/d\alpha$	void reactivity coefficient
$d\rho/dT_f$	fuel temperature reactivity coefficient
$\varphi_i(z)$	axial flux distribution in thermohydraulic region i
$\Sigma(r,z,t)$	3-D cross section
$\Sigma(z,t)$	1-D collapsed cross section
$\Pi(t,z)$	production operator
Π_0	linear component of the production operator
Π_1	nonlinear component of the production operator
λ_i	space eigenvalue of neutron diffusion equation
φ_i	i^{th} space eigenfunction of neutron diffusion equation (i^{th} harmonic)
φ_k	phase of the feedback transfer function at frequency k
A	core cross sectional area
D	diffusion coefficient
DR	decay ratio
F_{ave}	proportionality factor
H_k	gain of the feedback transfer function at frequency k
K	feedback gain; also reactivity eigenvalue
n or $n(t)$	time-dependent neutron density
n_i or $n_i(t)$	time-dependent neutron density for the ith neutron flux harmonic
N_b	number of bundles in core
N_i	number of bundles in thermohydraulic region i
N_{peak}	peak value of neutron density
N_{Th}	number of thermohydraulic regions used for a particular calculation
P_i	normalized power of thermohydraulic region i
P_{ij}	local power at axial node j in thermohydraulic region i
r	vector representing a particular position
T	oscillation period
T_f	fuel temperature
th	(subscript) thermal
V	core volume

NUREG/CR-6003
ORNL/TM-12130
NRC Category Distribution AN

INTERNAL DISTRIBUTION

1. J. March-Leuba
2. B. Damiano
3. H. R. Brashear
4. B. G. Eads
5. D. N. Fry
6. D. W. McDonald
7. D. R. Miller
8. R. E. Uhrig
9. J. O. Stiegler
10. D. G. O'Conor
11. C. E. Pugh
12. B. Chexal, Advisor
13. V. Radeka, Advisor
14. R. M. Taylor, Advisor

15-16. Central Research Library
17. Y-12 Technical Reference Section
18-19. Laboratory Records Department
20. Laboratory Records-Record Copy
21. ORNL Patent Section
22. I&C Division Publications Office

EXTERNAL DISTRIBUTION

23. D. E. Bessette, NLN-353, NRC/RES, Washington DC 20555
24. E. S. Beckjord, NLS-007, NRC/RES, Washington DC 20555
25. Amira Gill, WFN-8E23, NRC/NRR, Washington DC 20555
25. S. Fabic, MNBB-3701, AEOD/DOA, Washington DC 20555
26. W. S. Farmer, NLS-217B, NRC/RES, Washington DC 20555
27. T. L. Huang, WFN-8E23, NRC/NRR, Washington DC 20555
28. R. C. Jones, WFN-8E23, NRC/NRR, Washington DC 20555
29. T. E. Murely, WFN-12G18, NRC/NRR, Washington DC 20555
30. L. E. Phillips, WFN-8E23, NRC/NRR, Washington DC 20555
31. H. J. Richings, WFN-8E23, NRC/NRR, Washington DC 20555
32. B. W. Sheron, NL-007, NRC/RES, Washington DC 20555
33. H. H. Scott, NLN-353, NRC/RES, Washington DC 20555
34. L. M. Shotkin, NLN 353, NRC/RES, Washington DC 20555
35. A. C. Thadani, WFN-8E23, NRC/NRR, Washington DC 20555
36. NRC Central File
37. Assistant Manager for Energy Research and Development, DOE-OR, P.O. Box 2001, Oak Ridge, TN 37831-8600

38-47. Office of Scientific and Technical Information, U.S. Department of Energy, P.O. Box 62, Oak Ridge, TN 37831

NRC FORM 335 (2-89) NRCM 1102, 3201, 3202

U.S. NUCLEAR REGULATORY COMMISSION

BIBLIOGRAPHIC DATA SHEET

(See instructions on the reverse)

1. REPORT NUMBER (Assigned by NRC, Add Vol., Supp., Rev., and Addendum Numbers, if any.)

NUREG/CR-6003
ORNL/TM-12130

2. TITLE AND SUBTITLE

Density-Wave Instabilities in Boiling Water Reactors

3. DATE REPORT PUBLISHED

MONTH	YEAR
September	1992

4. FIN OR GRANT NUMBER

L1697

5. AUTHOR(S)

J. March-Leuba

6. TYPE OF REPORT

Technical

7. PERIOD COVERED *(Inclusive Dates)*

8. PERFORMING ORGANIZATION – NAME AND ADDRESS *(If NRC, provide Division, Office or Region, U.S. Nuclear Regulatory Commission, and mailing address; if contractor, provide name and mailing address.)*

Oak Ridge National Laboratory
Oak Ridge, TN 37831-6285

9. SPONSORING ORGANIZATION – NAME AND ADDRESS *(If NRC, type "Same as above"; if contractor, provide NRC Division, Office or Region, U.S. Nuclear Regulatory Commission, and mailing address.)*

Division of Systems Technology
Office of Nuclear Reactor Regulation
U.S. Nuclear Regulatory Commission
Washington, DC 20555

10. SUPPLEMENTARY NOTES

11. ABSTRACT *(200 words or less)*

This report contains a review of issues related to density-wave instabilities in boiling water reactors (BWRs). The report describes the types of instability modes that can be expected in operating reactors; these modes are (1) the channel thermo-hydraulic instability mode, (2) the core-wide instability mode, and (3) the out-of-phase instability mode. The physical mechanisms leading to each type of instability are reviewed and documented, along with some common mathematical models used in stability calculations. The main approximations used in these mathematical models are presented, and their impact on the accuracy of the calculations is reviewed. The linear behavior of a BWR is studied through the use of transfer functions, and the nonlinear behavior and limit cycle development are studied. A summary of the sensitivities to physical parameters is also included in this report.

12. KEY WORDS/DESCRIPTORS *(List words or phrases that will assist researchers in locating the report.)*

BWR instabilities
BWR stability
density-wave
limit cycle
power oscillations

13. AVAILABILITY STATEMENT

Unlimited

14. SECURITY CLASSIFICATION

(This Page)

Unclassified

(This Report)

Unclassified

15. NUMBER OF PAGES

16. PRICE